Coordination Chemistry Reviews 255 (2011) 1179–1205

Contents lists available at ScienceDirect

Coordination Chemistry Reviews

journal homepage: www.elsevier.com/locate/ccr

Review

Molybdenum enzymes in higher organisms

Russ Hille[a,*], Takeshi Nishino[a,b], Florian Bittner[c]

[a] Department of Biochemistry, University of California, Riverside, CA 92521, United States
[b] Department of Biochemistry and Molecular Biology, Nippon Medical School, 1-1-5 Sendagi, Bunkyo-ku, Tokyo, Japan
[c] Department of Plant Biology, Technical University of Braunschweig, 38023 Braunschweig, Germany

Contents

1. Introduction and scope 1180
2. Xanthine oxidoreductase 1181
   2.1. Introduction to structure 1181
   2.2. The reductive half-reaction 1182
   2.3. Active site residues 1184
   2.4. Intramolecular electron transfer 1187
   2.5. Biomedical aspects 1188
   2.6. ABA3 and sulfuration of xanthine oxidoreductase and aldehyde oxidase 1191
   2.7. Molybdenum cofactor insertion 1192
3. Aldehyde oxidase 1192
   3.1. Gene distribution in animals and higher plants 1192
   3.2. Protein structure and reaction mechanism 1193
4. Sulfite oxidase 1194
   4.1. Introduction to structures of plant and animal enzymes 1194
   4.2. The reductive half-reaction 1195
   4.3. Intramolecular electron transfer in chicken and human sulfite oxidase 1196
   4.4. The oxidative half-reaction 1197
   4.5. Pulsed EPR studies of sulfite oxidase 1197
5. Nitrate reductase 1199
   5.1. Introduction to structure 1199
   5.2. Kinetic behavior 1199
   5.3. Post-translational regulation 1201
6. Mitochondrial amidoxime reducing component 1201
   6.1. Substrates and distribution 1201
   6.2. The molybdenum centers of eukaryotic mARC enzymes 1202
7. Concluding remarks 1202
   Note added in proof 1203
   Acknowledgements 1203
   References 1203

ARTICLE INFO

Article history:
Received 17 September 2010
Accepted 20 November 2010
Available online 2 December 2010

Keywords:
Molybdenum enzymes
Xanthine oxidase
Sulfite oxidase
Nitrate reductase
hmARC

ABSTRACT

Recent progress in our understanding of the structural and catalytic properties of molybdenum-containing enzymes in eukaryotes is reviewed, along with aspects of the biosynthesis of the cofactor and its insertion into apoprotein.

* Corresponding author. Tel.: +1 951 827 6354.
E-mail addresses: russ.hille@ucr.edu (R. Hille), nishino@nms.ac.jp, takeshin@ucr.edu (T. Nishino), f.bittner@tu-bs.de (F. Bittner).

0010-8545/$ – see front matter © 2010 Elsevier B.V. All rights reserved.
doi:10.1016/j.ccr.2010.11.034

1. Introduction and scope

Molybdenum enzymes have long been recognized to be important in eukaryotes, dating to 1954 and the near-simultaneous demonstration of molybdenum in xanthine oxidase [1], aldehyde oxidase [2], and nitrate reductase [3]; molybdenum was subsequently identified as a component of sulfite oxidase in 1971 [4]. In the intervening time, and especially in the past decade, our understanding of the structures and function of these enzymes has developed to the point where it is possible to speak with confidence as to the precise manner in which the chemical transformations catalyzed by these enzyme occur and, in the context of high-resolution X-ray crystal structures, the specific means by which reaction rate is accelerated by these biological catalysts. At the same time, our understanding of the biosynthetic pathway by which the organic cofactor that accompanies molybdenum in eukaryotic systems is formed and the process by which molybdenum is incorporated and the resultant moiety inserted into apoprotein have all become increasingly well understood. Finally, new genomics and proteomics approaches continue to identify new molybdenum-containing proteins [5].

Historically, molybdenum enzymes from eukaryotes have been divided into two groups [6]: the xanthine oxidase family that includes the eponymous enzyme as well as the aldehyde oxidases; and the sulfite oxidase family, including both vertebrate and plant sulfite oxidases as well as the plant nitrate reductases. As indicated in Fig. 1, members of the xanthine oxidase family possess an $LMo^{VI}OS(OH)$ coordination sphere, where L is a pyranopterin cofactor that coordinates the metal via an enedithiolate side chain. (While the cofactor is frequently elaborated as a dinucleotide in prokaryotic enzymes, most frequently of guanine or cytosine, in all eukaryotic enzymes examined to date it is found as the mononucleotide shown in Fig. 1.) By contrast, the sulfite oxidases and nitrate reductase have an $LMo^{IV}O_2$(S-Cys) coordination sphere, with the cysteine ligand contributed by the polypeptide. Although both types of center possess a square-pyramidal coordination geometry with an apical Mo=O and three sulfurs and an oxygen in the equatorial plane, it has been pointed out that the orientation of the molybdenum coordination sphere with respect to the pyranopterin cofactor is opposite in the two families of protein [7]. With the pyranopterin group oriented to the left of the metal as shown in Fig. 2, the apical Mo=O points *up* for all members of the xanthine oxidase family, and *down* for all members of the sulfite oxidase family. In addition to these enzymes, several of which have been investigated for many years, a new protein catalyzing the oxidative hydroxylation of compounds such as amidoximes has recently been described in both humans and plants [8,9] which, as discussed further below, appears to have a distinct molybdenum coordination sphere and may represent a new family of eukaryotic molybdenum enzymes.

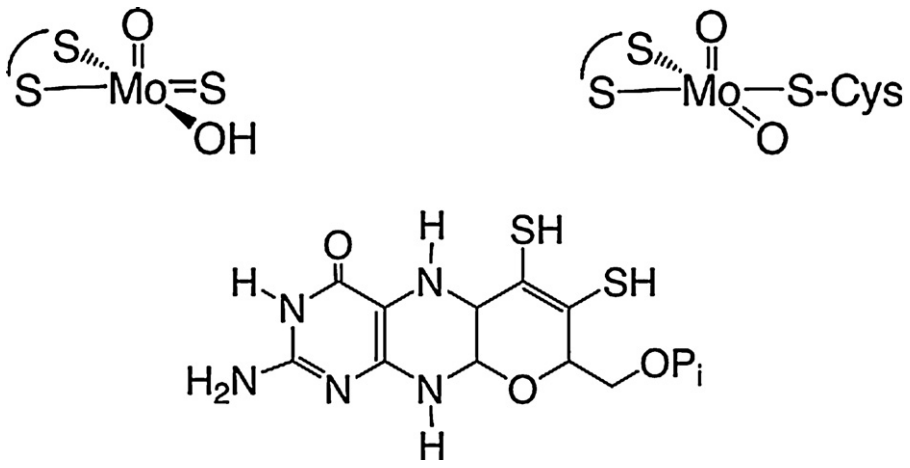

Fig. 1. Structures of the molybdenum centers of the xanthine oxidase and sulfite oxidase families of molybdenum enzymes. *Upper left*, the active site of bovine xanthine oxidase, *upper right*, the structure of chicken sulfite oxidase. Shown at *bottom* is the pterin cofactor (variously referred to in the literature as pyranopterin or molybdopterin) that coordinates the metal via its enedithiolate side chain.

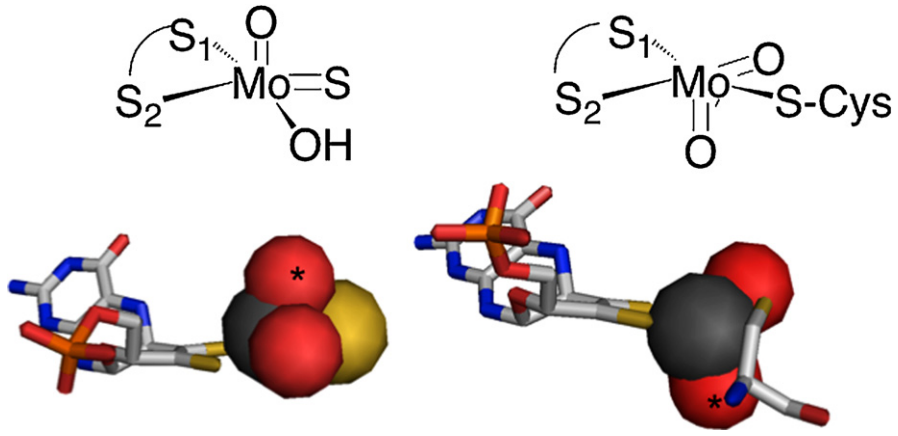

Fig. 2. The orientations of the molybdenum centers of xanthine oxidase and sulfite oxidase relative to the coordinated pyranopterin ligand. With the pyranopterin oriented as shown, the apical Mo=O (asterisk) of the molybdenum coordination sphere points up in all members of the xanthine oxidase family, and down in all members of the sulfite oxidase family.

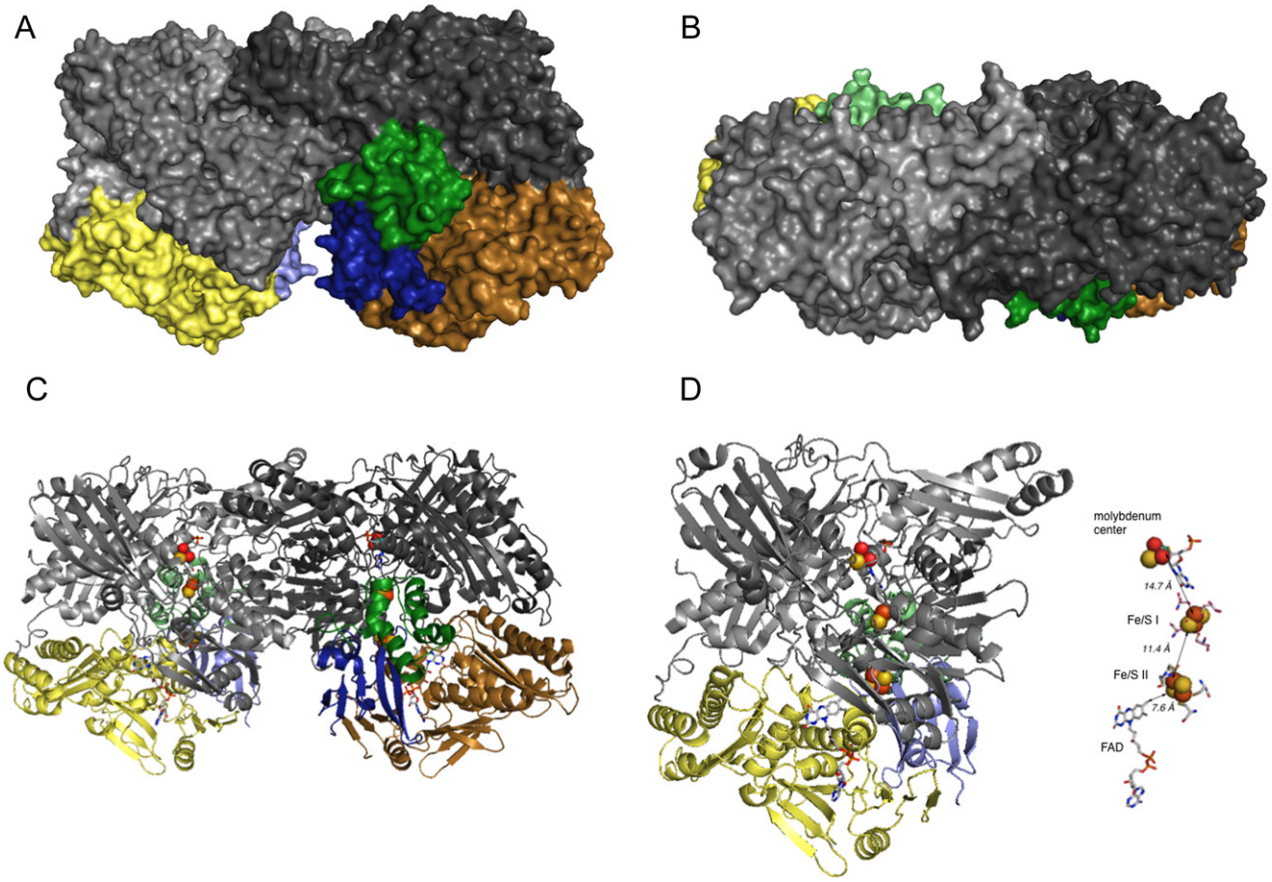

Fig. 3. The structure of bovine xanthine oxidoreductase. The iron–sulfur-containing domains are shown in blue and green, the FAD-containing domain in yellow, and the two domains that together constitute the molybdenum-binding portion of the protein are shown in gray. The two monomers are shaded in light and dark to distinguish them. A, a side view of the dimeric enzyme, in surface representation. B, top view, also in surface representation. C, a side view of the dimer in ribbon representation. D, a close-up of one monomer, with the approximately linear arrangement of the four redox-active centers shown at right. The edge-to-edge distances between adjacent redox-centers are given in Angstroms. The structure shown is based on the file 1FO4.pdb for the dehydrogenase form of the enzyme. All structures here and elsewhere are rendered using PyMOL.

The present account summarizes advances in our understanding of these systems, with an emphasis on more recent work dealing with structure–function relationships. The reader is referred to other reviews that focus on earlier work [6], and to accounts dealing with structural aspects of these enzymes [10], cofactor biosynthesis [7,11] and pulsed EPR applications [12] with perspectives different than that employed here.

2. Xanthine oxidoreductase

2.1. Introduction to structure

The X-ray crystal structures of xanthine oxidoreductase from bovine milk, in both its dehydrogenase and oxidase forms (utilizing NAD^+ and O_2, respectively, as substrate), were first reported by Enroth et al. in 2000 [13], and followed on the earlier report of the structure of the aldehyde:ferredoxin oxidoreductase from *Desulfovibrio gigas* [14], another member of the xanthine oxidase family of molybdenum enzymes. The overall structure of the homodimeric bovine protein as well as a close-up of the monomer is given in Fig. 3. Each monomer consists of five domains, from the N-terminus: two domains each with a [2Fe–2S] ferredoxin-like cluster, a first with principally β-sheet secondary structure and resembling the fold seen in spinach ferredoxin, and a second fold that is principally α-helical; a third domain that possesses FAD (this domain is absent in the *D. gigas* enzyme); and two large, C-terminal domains that together bind the active site molybdenum center at their interface. The subunit contacts in the dimer are entirely within the molybdenum-binding portion of the protein, but the molybdenum centers themselves are ~50 Å apart, indicating that the redox-active centers of the two monomers are well-insulated from one another. The polypeptide strand makes a single pass in going from one domain to the next, meaning that not only are the domains themselves autonomous structural elements of the polypeptide but that each domain is encoded by a contiguous stretch of the structural gene for the protein. Such a complex structure has obviously been built up from simpler elements over the course of evolution, as reflected by the fact that many bacterial enzymes of the xanthine oxidase family are $(\alpha\beta)_2$ or $(\alpha\beta)_2$ oligomers, with the Fe/S- and flavin-containing domains found in separate subunits from the molybdenum-binding portion of the protein.

Two aspects of the structure of the molybdenum center as inferred from the initial protein crystallography ultimately required revision. First, the Mo=S rather than Mo=O was initially considered to occupy the apical position of the molybdenum coordination sphere [14]. On the basis of the close similarity of the magnetic circular dichroism (MCD) of a catalytically relevant Mo(V) species (that giving rise to the so-called "very rapid" EPR signal, see below) and model compounds possessing an apical Mo=O, however, it was concluded that that the Mo=O must be apical in the enzyme [15]. This conclusion has subsequently been substantiated in the protein crystal structures of other members of this enzyme family, in particular the bacterial CO dehydrogenase [16]

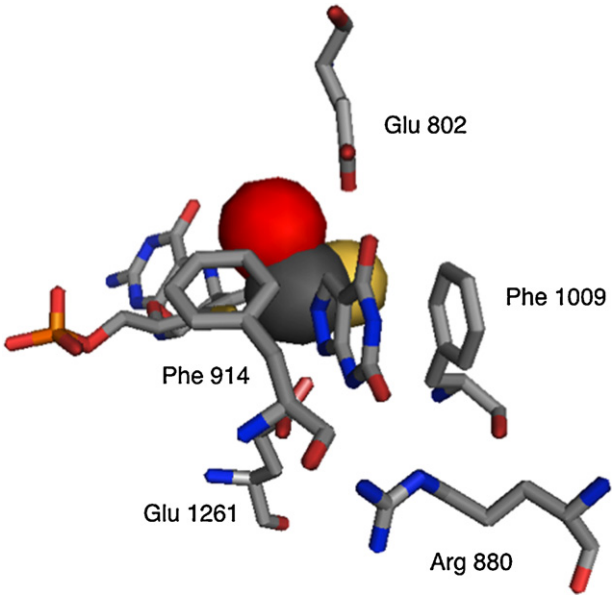

Fig. 4. The active site of bovine xanthine oxidase. Substrate binds between the Phe 914 and Phe 1009, with the plane of the substrate approximately parallel to the apical Mo=O bond. The remaining residues thought to play a prominent role catalytically are, clockwise from the top, Glu 802, Gln 767, Glu 1261 and Arg 880.

and quinoline 2-oxidoreductase [17], as well as that of xanthine oxidase itself trapped with the slow substrate FYX-051 [18]. It is now generally recognized that the Mo=O is apical in all enzymes of the xanthine oxidase family. Second, the equatorial oxygen ligand was initially thought to be water rather than hydroxide, but subsequent high-resolution X-ray absorption spectroscopy (XAS) has shown that at a distance of 1.98 Å the ligand is a hydroxide [19]. As discussed further below, the degree of protonation of the equatorial oxygen has mechanistic implications.

The oxidative hydroxylation of xanthine takes place at the molybdenum center of the enzyme, which on the basis of X-ray absorption spectroscopy studies [20,21] becomes reduced and protonated to an $LMo^{IV}O(SH)(OH)$ center in the course of the reductive half-reaction of the catalytic sequence. Electrons thus obtained are passed on to the FAD site, via the two iron–sulfur centers (Fig. 3D), prior to removal by either NAD^+ or O_2 (depending on whether the enzyme is in the dehydrogenase or oxidase form) in the oxidative half-reaction of the catalytic sequence. Fig. 4 shows the active site of xanthine oxidoreductase with several amino acid residues that are thought to be catalytically important. A 14.5 Å-long solvent access channel ends at a pair of phenylalanine residues (Phe 914 and Phe 1009 in the bovine enzyme) that constrain substrate to a plane parallel to the apical Mo=O group of the molybdenum center; the Mo–OH projects toward the substrate binding site. In addition to the two phenylalanine residues, four other active site residues are universally conserved in prokaryotic as well as eukaryotic xanthine oxidoreductases and dehydrogenases: Glu 802, Gln 767, Glu 1261 and Arg 880. These residues, with the molybdenum center itself, define the structural environment in which catalysis takes place.

The two iron–sulfur centers of xanthine oxidase have long been known to be distinguishable on the basis of their EPR signals [22]. The Fe/S I signal has $g_{1,2,3} = 2.022, 1.932, 1.894$, with unexceptional linewidths and relaxation properties for a [2Fe–2S] cluster, while Fe/S II has $g_{1,2,3} = 2.110, 1.991, 1.902$, with unusually broad linewidths and relaxation properties such that it observed only below 25 K [23]. Site-directed mutagenesis studies with a heterologously expressed rat xanthine oxidoreductase has made possible assignments of the two distinct EPR signals [24], with Fe/S I arising from the cluster in the unusual α-helical domain, and Fe/S II from the more normal ferredoxin-like domain. This assignment is consistent with the known coupling of Fe/S I to the molybdenum center, since this is the [2Fe–2S] cluster that is proximal to the molybdenum in the crystal structure [25,26].

2.2. The reductive half-reaction

It has been known for many years that water is the ultimate source of the oxygen atom incorporated into the hydroxyl group of product in the course of the reaction [27], but that a catalytically labile oxygen site on the enzyme exists that is the proximal donor of the hydroxyl group that is introduced into substrate [28]. This catalytically labile oxygen is the equatorial Mo–OH of the molybdenum coordination sphere [29], a conclusion subsequently substantiated by the protein crystal structure showing that the Mo–OH points toward the substrate binding site [13]. It had in fact been previously suggested on the basis of an examination of the properties of a series of inorganic model compounds to the enzyme active site that a Mo–OH might be catalytically labile [30]. Using the slow substrate 2-hydroxy-6-methylpurine [31], it was shown that the reaction proceeds through a reduced Mo(IV) species with product complexed to the molybdenum, which subsequently oxidized to a Mo(V) species giving rise to the catalytically relevant "very rapid" EPR signal; this latter species had long been recognized to contain product as part of the signal-giving species [32]. The structure of this EPR-active species has been examined by ESEEM [33], ENDOR [34,35] and finally crystallographically [36]; while the ENDOR data was initially interpreted as favoring a direct Mo–C bond in the signal-giving species [34], it is now clear that the signal-giving species is best formulated as $LMo^{V}OS(OR)$, with OR being product coordinated to the molybdenum via the catalytically introduced hydroxyl group in a simple end-on fashion [35,36]. The Mo(IV) species that precedes the EPR-active form in the catalytic sequence is thus $LMo^{IV}O(SH)(OR)$, where OR represents now-hydroxylated product (uric acid in the case of xanthine as substrate) coordinated to the molybdenum via the catalytically introduced hydroxyl group. The Mo–SH proton of the reduced center, while solvent-exchangeable, is initially derived from the C-8 position of xanthine that becomes hydroxylated [37].

The pH dependence for both the reductive half-reaction parameter k_{red}/K_d and the steady-state parameter k_{cat}/K_m of xanthine oxidoreductase is bell-shaped, reflecting ionizations with pK_as of 6.6 and 7.4 [38]. These parameters track the reaction of free enzyme with free substrate through the first irreversible step of the reaction, *i.e.*, formation of the $LMo^{IV}O(SH)(OR)$ species. The lower pK_a has been attributed to Glu 1261 acting an active site base analogously to the reaction mechanism proposed for the *D. gigas* aldehyde oxidoreductase [39], and the higher pK_a to substrate itself (reflecting the fact that enzyme works on the neutral rather than monoionic form of substrate) [40]. The reaction mechanism of xanthine oxidoreductase is thus thought to proceed as shown in Fig. 5 [6,29], via proton abstraction of the equatorial Mo–OH by the catalytic glutamate residue, with nucleophilic attack of the $Mo–O^-$ thus formed on the carbon to be hydroxylated and concomitant hydride transfer to the Mo=S group to give the initial $LMo^{IV}O(SH)(OR)$ intermediate. It is noteworthy that earlier work with a homologous series of substituted quinazolines had in fact suggested that the reaction mechanism involved nucleophilic attack on substrate [41]. That the catalytically labile oxygen is initially an Mo–OH is important, since the deprotonated $Mo–O^-$ is expected to be a much better nucleophile than a Mo–OH obtained by deprotonation of a $Mo–OH_2$ [19].

The initially formed $LMo^{IV}O(SH)(OR)$ intermediate breaks down by displacement of product from the molybdenum coordination sphere by hydroxide from solvent, with electron transfer from the molybdenum to the other redox-active centers of the enzyme and

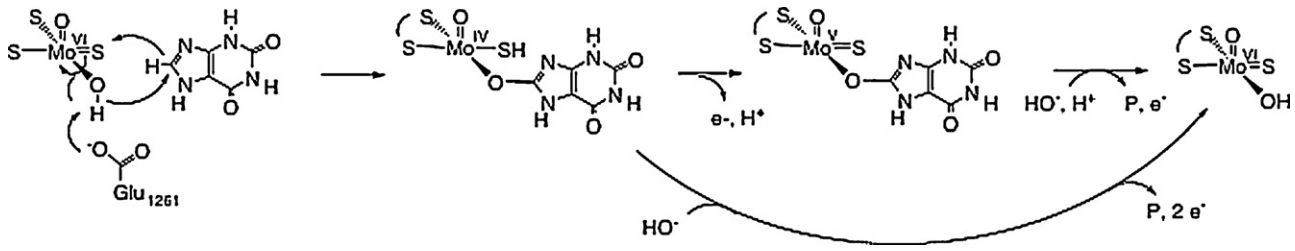

Fig. 5. The reaction mechanism of xanthine oxidase. Catalysis is thought to be initiated by base-assisted nucleophilic attack of the equatorial Mo–OH of the molybdenum coordination sphere on the C-8 position of substrate, with hydride transfer to the equatorial Mo=S group to give an initial $LMo^{IV}O(SH)(OR)$ intermediate. Depending on the reaction conditions, as discussed in the text, this intermediate breaks down by electron transfer to the other redox-active centers of the enzyme and deprotonation to yield a Mo(V) species giving rise to the "very rapid" EPR signal, or by hydroxide displacement of product from the molybdenum coordination sphere, followed by rapid electron transfer out of the molybdenum center.

deprotonation of the Mo–SH to return to the Mo=S of oxidized enzyme. The sequence in which these events occur depends on the reaction conditions and the substrate utilized – when partial reoxidation precedes displacement of substrate, the "very rapid" $LMo^{V}OS(OR)$ species is formed. Under most conditions, however, product dissociation precedes electron transfer out of the molybdenum center and the "very rapid" species is by-passed. It has been shown with both the bovine and chicken enzymes that product dissociation is predominantly rate-limiting in the reductive half-reaction, and the first step of the reaction (leading to the $LMo^{IV}O(SH)(OR)$ intermediate) is faster by a factor of approximately 75 [42]. It is also important to bear in mind that formation of the "very rapid" species, when it does from, is an oxidative event from the standpoint of the molybdenum center, and that the initial intermediate is formally a Mo^{IV} species. Although it has been suggested that the Mo^{V} species might be formed directly by direct one-electron transfer from substrate [43], the lack of correlation between reduction potential and reaction rate in a homologous series of substituted purines indicates that this is not likely to be the case [44].

Notably absent from the catalytic sequence is the species giving rise to the "rapid" EPR signal (actually, a family of closely related signals [45–47]) that appear on a slower time scale than the "very rapid" signal and were long thought to arise from an intermediate lying downstream from the "very rapid" species in the catalytic sequence. It has been shown, however, that this signal possesses bound substrate rather than product, and can be formed very rapidly and noncatalytically simply by binding substrate to enzyme that has been partially pre-reduced by titration with sodium dithionite [48]. Although technically a dead-end intermediate from a kinetic standpoint (the molybdenum center cannot react with substrate until fully reoxidized to the Mo(VI) state), the "rapid" species is perhaps best thought of as a paramagnetic analog to the Michaelis complex of the enzyme.

On the basis of a detailed consideration of the non-Arrhenius behavior of the temperature dependence for the limiting rate constant for enzyme reduction at high concentrations of xanthine, it has proven possible to obtain values for the microscopic rate constants for formation and decay of the key $LMo^{IV}O(SH)(OR)$ intermediate of the reductive half-reaction as a function of temperature, and determine the entropy and enthalpy of activation for each step [49]. In particular, formation of the intermediate is marked by a large negative entropy of activation (-70 cal mol^{-1} deg^{-1}), reflecting a highly ordered transition state such as might be expected on the basis of the likely concerted nucleophilic attack/hydride transfer chemistry involved. Interestingly, this leads to a situation where the relative rate constants for formation and decay of this intermediate reverse over the temperature range 15–50 °C; at lower temperatures breakdown of the $LMo^{IV}O(SH)(OR)$ intermediate by product dissociation is rate-limiting (consistent with the results of the isotope effect study referred to above [42] indicating that the chemical step of the reaction is not rate-limiting), but that at higher temperatures its formation becomes rate-limiting.

The reaction of models for the molybdenum center of xanthine oxidase with substrates and substrate analogs has been examined computationally by several groups, employing density functional theory (DFT). The first study provided computational support for a mechanism such as that described above involved a study of the reaction of an $LMo^{VI}OS(OH)$ complex (with L being butene-2,3-dithiolate) as a model for the active site and formamide as substrate (the enzyme is in fact able to hydroxylate formamide to carbamate) [50]. In this work, a reaction involving nucleophilic attack on the substrate carbon, $sp^2 \rightarrow sp^3$ rehybridization and finally hydride transfer was found to lie to considerably lower energy than one involving insertion of the C–H bond of substrate across the Mo=S to give an intermediate with a direct Mo–C bond, as had been previously suggested [34]. Further work provided insight as to the basis for the catalytic requirement for an equatorial Mo=S. Working with the same model and formamide as in the earlier study, it was shown that substitution of a second, equatorial Mo=O for the Mo=S of the original model resulted in a 15 kcal/mol increase in the energy of the transition state in a nucleophilic attack mechanism [51], more than sufficient to account for the loss of catalytic activity observed experimentally when the sulfur is lost [52]. Interestingly, substitution of tellurium for sulfur lowered the transition state energy by 3 kcal/mol, suggesting that a tellurium- or selenium-substituted form of the enzyme might exhibit even more activity as the native form. (A selenium-containing member of the xanthine oxidase family of enzymes, nicotinate dehydrogenase from the anaerobic soil bacterium *Eubacterium barkerii*, has recently been characterized crystallographically and the reactivity of its $LMo^{VI}OSe(OH)$ active site examined computationally [53].) The high covalency of the Mo=S (or, presumably to an even greater degree, Mo=Se) is principally due to the π rather than σ interaction between the in-plane ligand p orbital and the redox-active d_{xy} of the molybdenum [54,55]. This covalency has the effect of substantially delocalizing the Mo d_{xy} orbital onto the sulfido group, effectively increasing its electrophilicity relative to an oxo group and enhancing its reactivity as a hydride acceptor.

Subsequent computational work has probed whether nucleophilic attack and hydride transfer are concomitant, or whether the reaction leading to the $LMo^{IV}O(SH)(OR)$ species passes through a discrete sp^3-hybridized intermediate. With aldehydes as substrate, DFT calculations suggest that a concerted mechanism represents the lowest-energy pathway for the reaction, while with formamide as substrate (which is intrinsically less reactive toward nucleophilic attack) a pathway involving a discrete sp^3-hybridized intermediate occupying a local minimum along the reaction coordinate is slightly preferred [56]. It was also shown that strategically placed water molecules (possibly mimicking amino acid residues in the enzyme active site that could not be effectively included in the model used in the calculations) greatly facilitated the reaction by

stabilizing negative charge accumulation on substrate in the course of the nucleophilic attack. In subsequent work explicitly incorporating the active site glutamate thought to act as a general base, a concerted mechanism was considered more likely [57].

In an effort to more realistically incorporate enzyme structural information into the computational models, a combined QM/MM approach has been taken, in which the chemical transformations in the active site are dealt with quantum mechanically, while active residues not directly involved in bond making and breaking are treated using molecular mechanics to keep the calculations manageable [58,59]. A large number of combinations of tautomeric forms for xanthine as substrate, ionization states of active site residues and alternate substrate orientations have been explicitly considered, and in all cases the lowest-energy course of the reaction proceeds via base-assisted nucleophilic attack [58]. The precise manner in which specific amino acid residues contribute to transition state stabilization depends critically on their ionization state and the orientation of substrate in the active site. It was concluded that the most lowest-energy pathway involves an orientation of substrate with its "distal" C_2=O oriented toward the active site Arg 880, with Glu 802 protonated and hydrogen bonding to the "proximal" C_6=O [58]. In comparing the barrier heights for the several reaction pathways, however, the authors did not consider the free energy required to populate their preferred orientation, which their own calculations determined to be less stable than one in which substrate is oriented in the opposite direction, with the C_6=O oriented toward Arg 880 instead (see below) – the free energy required to reorient substrate for more "favorable" reaction should properly be counted as part of the energetic cost of attaining the transition state. A more detailed treatment of computational approaches to the reaction mechanism of xanthine oxidase and related enzymes is considered elsewhere in this issue [60].

2.3. Active site residues

Mutagenesis studies of several of the amino acid residues shown in Fig. 4 have been undertaken in the past several years. The first work utilized a heterologous expression system of the *Rhodobacter capsulatus* xanthine dehydrogenase in *Escherichia coli* and focused on Glu 232 (corresponding to Glu 802 in the bovine enzyme) and Glu 730 (corresponding to Glu 1261) [61]. Mutation of Glu 232 to alanine reduced k_{cat} in steady-state experiments from 108 s^{-1} to 4.4 s^{-1}, and k_{red} in the anaerobic reduction of enzyme by xanthine from 67 to 5.5 s^{-1}; in the latter experiments, K_d increased from 34 μM to 409 μM, reflecting compromised affinity of substrate for the active site with the mutation. The effect on k_{red} and K_d from the rapid reaction work indicates that the interaction between Glu 232 and substrate provides ~3 kcal/mol of free energy, approximately half of which is utilized by the enzyme stabilize the transition state (as reflected in the lower k_{red} exhibited by the mutant) and half to bind substrate (as reflected in the higher K_d seen in the mutant). However, given that the chemical step of the reaction may well have become rate-limiting in the mutant (while in wild-type enzyme it probably is not, by a factor of ~75 by analogy to the vertebrate enzymes) the actual free energy available from the interaction may be as great as ~5.5 kcal/mol, of which only 1.5 kcal/mol is utilized to simply bind the substrate. Studies of an E803V mutant of the *E. coli*-expressed human xanthine oxidoreductase exhibits a reduction in k_{cat} from 18 s^{-1} to 1.3 s^{-1} and an increase in K_m from 8.8 μM to 72 μM [62], consistent with the results with the bacterial enzyme.

The putative active site base Glu 730 (Glu 1261 in the bovine enzyme) has also been changed to Ala, Asp, Gln and Arg [61]. In no case was activity detected in steady-state assays, neither were any of the mutants reduced to any appreciable degree by 100 μM xanthine under anaerobic conditions, even in an overnight incubation. Even taking into account the variable amount of functional molybdenum center in the mutants (33–60% in the mutants, as compared with 76% in the wild-type enzyme), the loss of activity was profound and it was estimated that k_{red} has been compromised by at least a factor of 10^7 [61]. The implication is that Glu 730/1261 contributes at least 10 kcal/mol toward transition state stabilization in the enzyme-catalyzed reaction.

Finally, Arg 310 (Arg 880 in the bovine enzyme, and Arg 881 in the human) has been mutated to Lys and Met [63]. While this residue is more than 8 Å away from the molybdenum, the principal effect of the mutation is a 2000-fold reduction in k_{red}, to 0.002 s^{-1}, indicating that Arg 310 contributes significantly to transition state stabilization, by at least 4.5 kcal/mol. An R310K mutant exhibits a much more modest reduction in k_{red}, to 1.6 s^{-1}. In separate work published at the same time, mutation of Arg 881 in the human enzyme has no detectable activity in steady-state assays [62]. The loss of reactivity toward xanthine notwithstanding, the R881M mutant of the human enzyme had considerably *more* reactivity toward benzaldehyde as substrate, with both a two-fold lower K_m and three-fold higher k_{cat} as compared to wild-type enzyme [62]. Arg 881 is not conserved in the otherwise closely related aldehyde oxidases (see below), and it is evident that this reside confers substrate specificity that distinguishes the two subfamilies of enzyme.

On the basis of the above, it is evident that Glu 802, Glu 1261 and Arg 880 (in the bovine enzyme) all contribute to rate acceleration in the reaction catalyzed by xanthine oxidase, Glu 1261 profoundly so, and the question is how specifically they do so. Glu 1261 is widely considered to act as an active site base as discussed above [38,39]. On the basis of the calculated relative stabilities of several tautomers of free xanthine and the purine ring in the $LMo^{IV}O(SH)(OR)$ intermediate, it has been suggested that Glu 232 accelerates reaction rate specifically by facilitating a tautomerization of the heterocycle in the course of nucleophilic attack that involves proton transfer from N_3 to N_9 of the purine ring and serves to compensate for the negative charge accumulating on the imidazole subnucleus of the purine in the course of the reaction [64], as illustrated in Fig. 6, Top. With regard to Arg 880, it has been suggested that this residue is also involved in stabilizing negative charge accumulation on the heterocycle in the course of nucleophilic attack by interacting with the "proximal" C-6 carbonyl of the pyrimidine subnucleus of substrate, as shown in Fig. 6, Bottom. The proposed roles proposed for Glu 802 and Arg 880 depend critically on the orientation of substrate in the active site. With the purine ring constrained by Phe 914 and 1009 to a plane parallel to the apical Mo=O, two orientations are possible as shown in Fig. 7A. In the first orientation, Glu 802 and Arg 880 are positioned to function as described above, and to bind as shown in the second orientation compromises their contribution to transition state stabilization and rate acceleration. Indeed, in a homologous series of purine substrates (all hydroxylated at same position as is xanthine) substrates fell into two groups on the basis of their structures and reactivity with xanthine oxidase: effective substrates for wild-type enzyme (including xanthine) that had a C_6=O or C_6=S group were profoundly affected by the R310M mutation, while poorer substrates for wild-type enzyme without such a group were minimally affected by the mutation [63]. It was proposed that the poor substrates lacking a functional group able to interact effectively with Arg 880 bound in the less effective orientation, accounting for why they were not affected by mutation Arg 880 to Met.

The first crystallographic evidence as to substrate orientation in the active site came from the structure of the reduced *R. capsulatus* xanthine dehydrogenase in complex with alloxanthine, a mechanism-based inhibitor of xanthine oxidoreductase that has long been known to form a very stable complex with the reduced form of the enzyme [65]. In the crystal structure [66], alloxanthine is oriented in the active site as shown in Fig. 7B, with a direct bond between N-2 of the pyrazole subnucleus of the inhibitor and

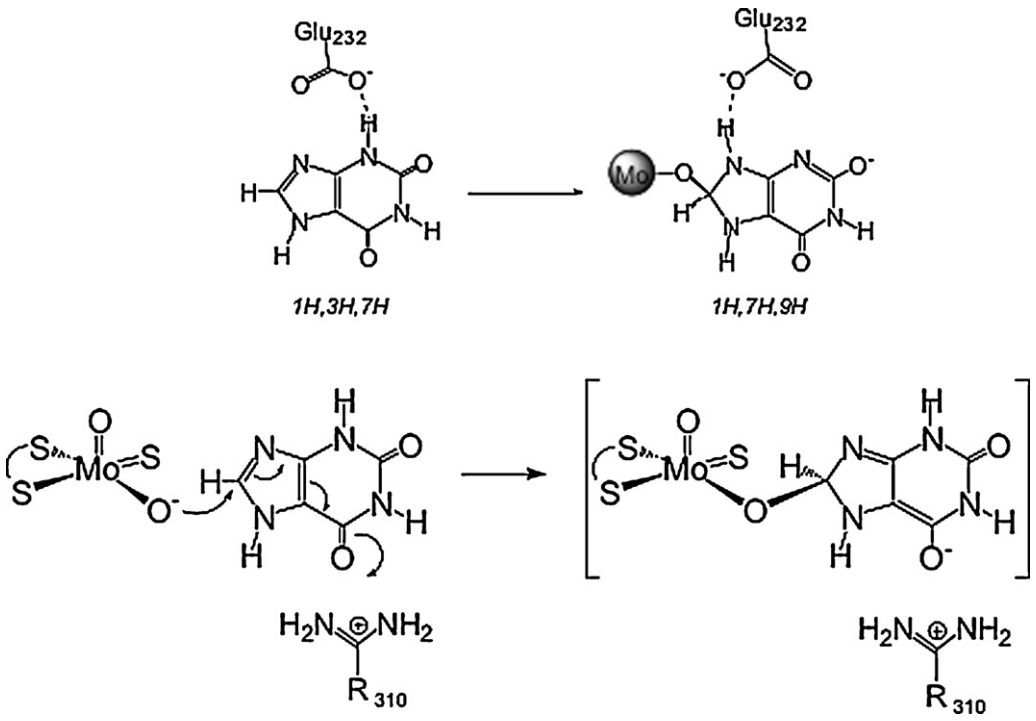

Fig. 6. Proposed catalytic roles for Glu 802 and Arg 880. Top, Glu 802 serving to facilitate tautomerization of the heterocycle in the course of nucleophilic attack [61]. Bottom, Arg 880 serving to stabilize negative charge accumulation on the heterocycle in the course of the reaction [63].

the molybdenum, and the pyrimidine subnucleus oriented with its "distal" keto group pointing toward Arg 310. In the structure, however, there is a direct bond between the pyrazole nitrogen and metal, and the heterocycle thus sits closer to the molybdenum in the active site than would substrate in the Michaelis complex. The question is whether in the somewhat more removed position likelier for bound substrate in the Michaelis complex, the more stable configuration is inverted compared to that seen in the alloxanthine-complexed enzyme, with the "proximal" rather than "distal" keto group of the pyrimidine subnucleus interacting instead with the active site arginine.

Subsequently, X-ray crystal structures of the bovine enzyme in complex with a variety of substrates and substrate analogs have been examined in an effort to address the issue of substrate orientation in the active site. With the poor substrate 2-hydroxy-6-methylpurine, the structure shown in Fig. 7C is seen (at a resolution of 2.3 Å) [36], with clear bridging electron density between the molybdenum and C-8 of the heterocycle, reflecting progression through the catalytic sequence to the $LMo^{IV}O(SH)(OR)$ intermediate or its $LMo^{V}OS(OR)$ oxidation product (probably the latter since the observed Mo–S distance of 2.0 ± 0.2 Å suggesting a Mo=S rather than Mo–SH ligand, for which a distance on the order of 2.4 Å would be expected). The orientation of substrate, and in particular the Mo···C distance of 3.4 Å, are consistent with the ESEEM [33] and ENDOR [35] studies of the "very rapid" Mo(V) species. The asymmetry of the electron density for the coordinated product (2,8-dihydroxy-6-methylpurine) in the active site clearly indicates that it is oriented with the "distal" keto group of the pyrimidine subnucleus toward Arg 880, and is within hydrogen-bonding distance of it at 3.1 Å. 2-hydroxy-6-methylpurine is a poor substrate for xanthine oxidase and the observed orientation has been interpreted as being that of the less effective catalytic orientation shown in Fig. 7A.

The nonfunctional desulfo form of the enzyme in complex with xanthine (originally at 2.6 Å resolution, Fig. 7D), and of the functional form in reaction with the pteridine substrate lumazine (originally at 2.2 Å resolution, Fig. 7E) have also been reported [67]. Both these heterocycles are "good" substrates and in both structures the orientation of the pyrimidine subnucleus is opposite that seen with the poor substrate 2-hydroxy-6-methylpurine, with the "proximal" rather than "distal" keto group oriented in each case toward the active site Arg 880. It has been concluded that this represents the more catalytically effective orientation on the basis of the argument above. Both structures have been subsequently been resolved to better than 1.8 Å resolution, and the asymmetric electron density of substrate remains clearly defined. It has been concluded (controversially, see below) that purine substrates do indeed bind to xanthine oxidase in two different ways, with the more catalytically effective orientation such that Glu 802 is indeed positioned appropriately to function catalytically in facilitating tautomerization between N-3 and N-9, and Arg 880 by stabilizing negative charge accumulation on the C-6 carbonyl of substrate in the course of nucleophilic attack.

An alternative interpretation to the above mutagenesis work is that purine substrates always bind with the pyrimidine ring oriented as seen in the crystal structure of enzyme in complex with alloxanthine. While the chemical course of the reaction is identical to that shown in Fig. 5, the several active site residues are assigned different roles in substrate binding and rate acceleration. In such an orientation (Fig. 8), Glu 802 cannot be involved in protonating the imidazole subnucleus of the heterocycle, and it has been suggested instead that Glu 1261 dos so after having abstracted the Mo–OH proton [62]. Glu 802 is instead proposed to be protonated and hydrogen bonding to the proximal C-6 carbonyl group of substrate. This alternate interpretation is supported by the QM/MM work described above [58], but again the question is whether the relative activation barriers for the two substrate orientations were properly gauged in this work.

Xanthine oxidase not only hydroxylates xanthine at C-8 to give uric acid, but also hypoxanthine at C-2 to give xanthine. The role of amino acid residues in catalysis of C-2 has been probed in an examination of the crystal structures of bovine xanthine oxidase in complex with hypoxanthine (at 1.8 Å resolution) and the

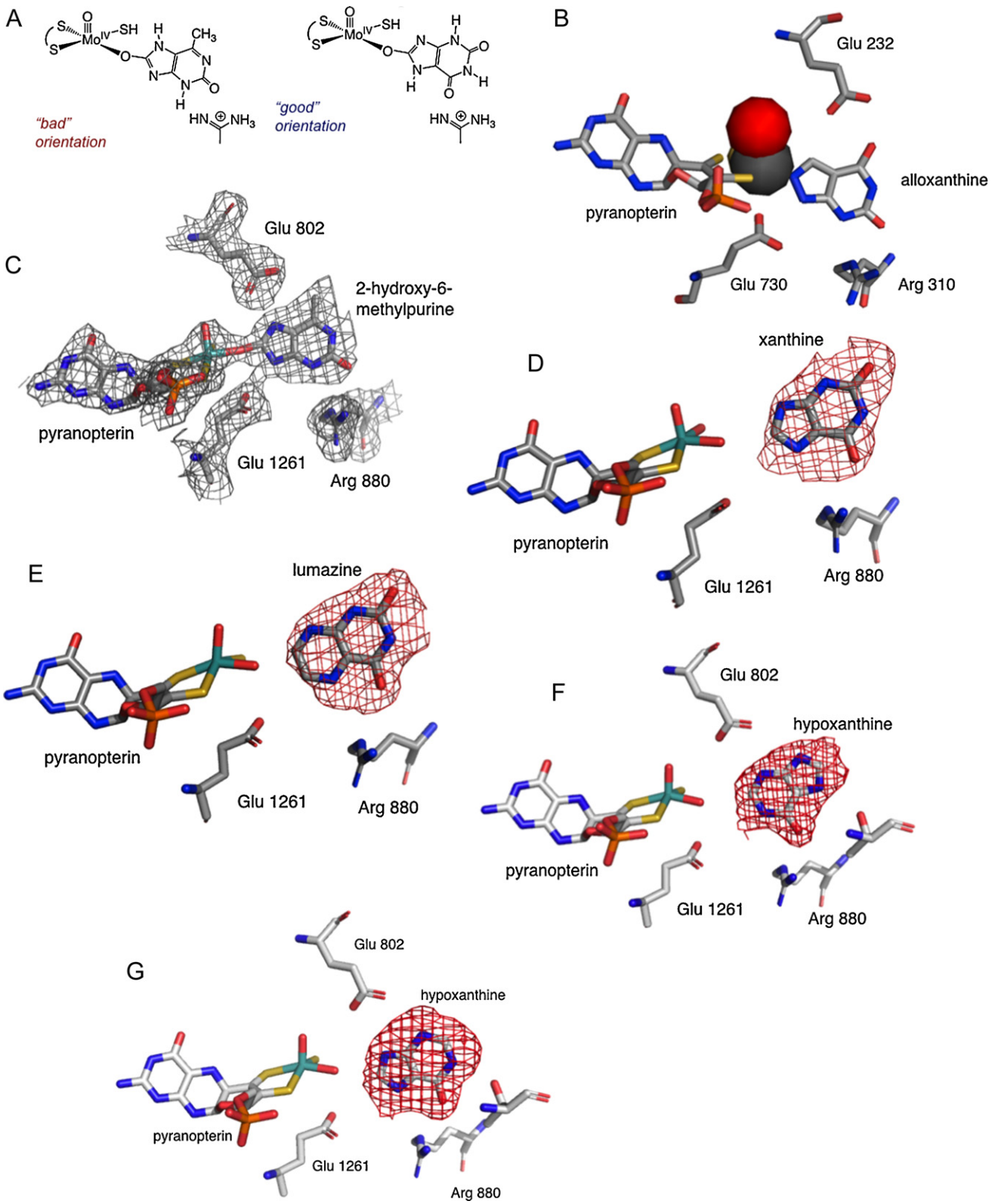

Fig. 7. Substrate orientation in the active site of xanthine oxidase. A, schematic diagrams for the catalytically less effective (left) and more effective (right) orientations of substrate in the enzyme active site; B, the structure of xanthine dehydrogenase of *Rhodobacter sphaeroides* with alloxanthine complexed to the molybdenum center (prepared from PDB file 1JRP, [66]); C, the structure of the functional form of the bovine xanthine oxidase in the course of reaction with the slow substrate 2-hydroxy-6-methylpurine [36]; D, the structure of the nonfunctional, desulfo form of bovine xanthine oxidase with xanthine bound in the active site [67]; E, the structure of functional bovine xanthine oxidase in the course of reaction with lumazine [67]; F and G, the structure of functional bovine xanthine with hypoxanthine, with substrate oriented with C-2 and C-8 toward the molybdenum center, respectively [68].

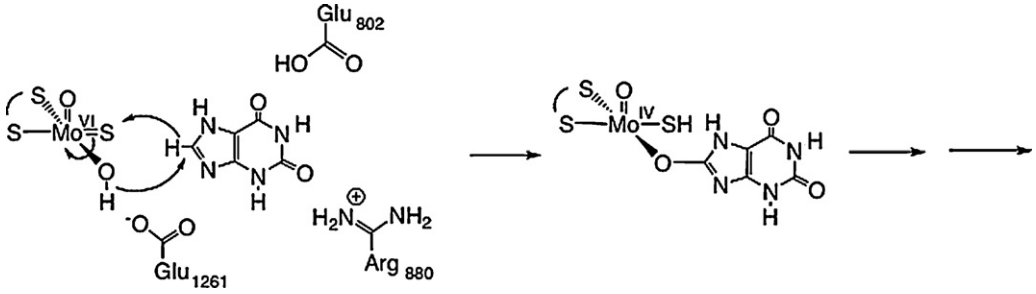

Fig. 8. Alternate roles for active site residues of bovine xanthine oxidase in accelerating catalysis. With substrate oriented as shown, Glu 1261 serves to simultaneously deprotonate the equatorial Mo–OH and protonate the imidazole subnucleus of substrate in the course of nucleophilic attack. Glu 802 is protonated and hydrogen-bonds to the C_6=O carbonyl of substrate, and Arg 880 interacts with the C_2=O carbonyl.

chemotherapeutic agent 6-mercaptopurine (at 2.6 Å resolution) [68]. For each substrate, different orientations are observed in the two active sites of the crystallographic asymmetric unit (containing one protein dimer). One orientation is appropriate for hydroxylation at C-2 of substrate, leading to xanthine or 6-thioxanthine as product (Fig. 7F), the other has C-8 oriented toward the active site molybdenum center (Fig. 7G), as if to give 6,8-dihydroxypurine. Kinetic work done in conjunction with the crystallography has demonstrated that hypoxanthine is hydroxylated essentially quantitatively at C-2, indicating that if hypoxanthine does indeed bind in an orientation that permits hydroxylation at C-8 the reaction must proceed only very slowly [68]. The apparent enzyme selectivity for C-2 over C-8 with hypoxanthine has been attributed to a combination of relatively subtle differences in substrate orientation in the active site and differences in the intrinsic reactivity of the two sites [68]. This work also demonstrated that the preferred tautomer of hypoxanthine with N-9 of the imidazole subnucleus is (modestly) more stable than that with N-7 protonated. This being the case, Glu 802 is positioned as shown in Fig. 9 to facilitate tautomerization and negative charge stabilization in the course of nucleophilic attack, this time from N-9 to N-3 (the reverse sense as proposed in the hydroxylation of xanthine at C-8). Similarly, Arg 880 is positioned to again stabilize negative charge accumulation. A comparison of the effects of mutation of Glu 803 and Arg 881 of human xanthine oxidoreductase with xanthine and hypoxanthine as substrate indicates that Arg 881 plays the more important role with xanthine as substrate, but Glu 803 has the greater role catalytically with hypoxanthine as substrate [62].

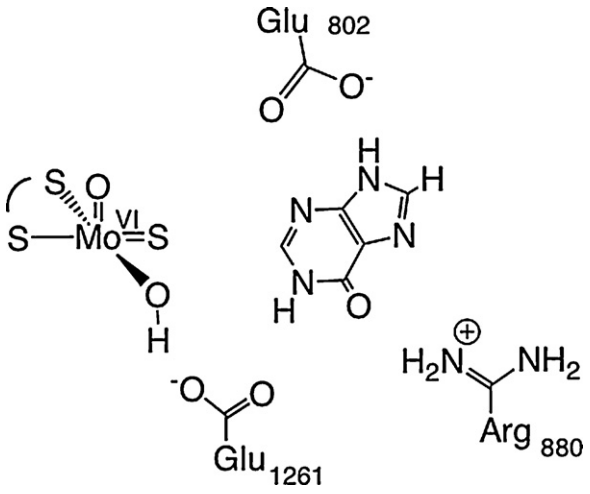

Fig. 9. Proposed roles of Glu 802 and Arg 880 in the hydroxylation of hypoxanthine. With substrate oriented for hydroxylation at the C-2, Glu is positioned to facilitate proton tautomerization from the imidazole to the pyrimidine subnucleus (*left*), and Arg 880 to interact with the C_6=O carbonyl (*right*).

2.4. Intramolecular electron transfer

Because reducing equivalents enter xanthine oxidoreductase at its molybdenum center and depart via the flavin, it has long been recognized that intramolecular electron transfer is an integral aspect of turnover, and the distribution of reducing equivalents among the enzyme's four redox-active centers assumed to be rapid and determined by their relative reduction potentials [69]. Electron transfer within the bovine enzyme has been examined by both pH-jump [70,71] and pulse radiolysis [72,73] methods. In the former studies, advantage is taken of the greater pH dependence of the FAD and molybdenum reduction potentials relative to the iron–sulfur clusters to perturb the distribution of reducing equivalents among the several centers simply by mixing partially reduced enzyme in dilute buffer at one pH with more concentration buffer at another (under strictly anaerobic conditions). It was observed that the rate of equilibration between the iron–sulfur clusters (principally Fe/S I) and FAD increases monotonically from 155 s^{-1} at pH 6 to 330 s^{-1} at pH 9 (with iron–sulfur reduction favored at the higher pH); the activation energy for the equilibration process observed decreased from 19.8 kcal/mol to 8.7 kcal/mol over the same pH range [70]. The observed solvent kinetic isotope effect on the observed equilibration was subsequently determined to be large, 6.9, and the linear dependence of the observed rate constant on mole fraction of D_2O indicated that the effect involved a single proton [71]. Given the known relative reduction potentials of the centers involved (from which the ratio of the microscopic forward and reverse rate constants could be determined) and the observed rate constant for equilibration of reducing equivalents (representing the sum of the forward and reverse rate constants) it was possible to calculate the forward and reverse rate constants explicitly in both H_2O and D_2O, with the finding that the isotope effect was much larger for the $FADH^{\bullet} \rightarrow$ Fe/S I_{ox} electron transfer event rather than the reverse process. It was concluded that the N_5-H proton of the neutral flavin semiquinone was in motion as the system traversed the electron-transfer transition state, meaning that electron and proton transfer were concomitant – this was attributed to the destabilization of the $FAD^{\bullet -}$ anionic semiquinone by the protein environment, meaning that protonation prior to electron transfer was thermodynamically unfavorable [71]. Approximately half of the statically observed spectral change was observed kinetically in these pH jump experiments, with calculations indicating that a second equilibration involving Fe/S I and the molybdenum center occurred in the 1 ms dead-time of the stopped-flow apparatus. In subsequent pulse radiolysis studies, electrons were rapidly introduced into the enzyme using radiolytically generated methylnicotinamide radical at the molybdenum center [72]. At pH 6.0, rapid electron transfer to the iron–sulfur centers occurred with a rate constant of 8500 s^{-1}, with a subsequent process associated with electron transfer from the iron–sulfur centers on to the flavin at 125 s^{-1} (in good agreement with the pH jump work). The observation of Mo → Fe/S → FAD elec-

tron transfer in the protein was subsequently substantiated with the X-ray crystal structure of the protein, which showed the two iron–sulfur centers intervening between the molybdenum center and FAD.

The behavior of xanthine oxidase in pH jump experiments, implicating concomitant electron/proton transfer involving the iron–sulfur centers and FAD, contrasts with that exhibited by other flavin- and iron/sulfur-containing systems such as trimethylamine dehydrogenase (which contains a [4Fe–4S] iron–sulfur cluster and a covalently linked FMN [73]). In this protein, while the observed solvent isotope effect on intramolecular equilibration is again large, a plot of the observed rate constant versus mole fraction D_2O indicates the involvement of multiple protons in the electron transfer event [74]. Furthermore, reductive titrations over the pH range 6–10 provide clear evidence for uncoupling of the protonation/deprotonation equilibria with the electron transfer event, and taking explicitly into account the $FMNH_2 \rightleftharpoons FMNH^-$ and $FMNH^\bullet \rightleftharpoons FMN^{\bullet -}$ ionizations it is possible to accurately reproduce the rather complicated pH dependence of the observed rate constant for redox-equilibration assuming intrinsically very rapid electron transfer over the 4.5 Å separating the two redox-active centers [73]. The different behavior of trimethylamine dehydrogenase and xanthine oxidase has been attributed to the fact that the former does not thermodynamically destabilize the anionic forms of the flavin, allowing deprotonation to precede electron transfer out of the flavin [75].

2.5. Biomedical aspects

Xanthine oxidoreductase catalyzes two hydroxylation steps of the purine degradation metabolic pathway, *i.e.*, hypoxanthine to xanthine and xanthine to uric acid, utilizing either NAD^+ or O_2 [47], and as indicated above, it occurs in two forms: xanthine dehydrogenase, which prefers NAD^+ as the substrate, and xanthine oxidase, which prefers O_2 [76,77]. Historically, the dehydrogenase and oxidase have been studied as distinct enzymes. The oxidase form is typically isolated from mammalian sources, such as cow's milk [78,79], whereas the dehydrogenase form is obtained from other organisms, such as chicken [80,81], insects [82] and bacteria [6,66]. It is clear, however, that even the mammalian enzyme exists predominantly as the dehydrogenase form under normal physiological conditions in the cell, but can be converted to the oxidase form during extraction or purification, either irreversibly by proteolysis or reversibly by oxidation of cysteine residues to disulfide bonds [83–87]. In some cases, xanthine dehydrogenase from other organisms can be reversibly converted to the oxidase form [88–91]. The mechanism of the dehydrogenase:oxidase conversion has been thoroughly elucidated in the past decade by means of a range of techniques, including X-ray crystal structure analysis of various mutants, and it has become clear that the protein environment influences the reactivity of the FAD toward different substrates through substantial conformational changes triggered by modifications located far from the cofactor [92]. This conversion is mechanistically highly sophisticated, as will be described below, suggesting that it is not simply an artifact but rather is physiologically significant. An important physiological role for mammalian xanthine oxidoreductase in milk secretion is suggested by the results of gene knockout experiments, in which otherwise healthy female mice are seriously dysfunctional in lactation [93]. As the conversion from dehydrogenase to oxidase occurs only in mammals, and most of the enzyme in secreted mouse milk is in the oxidase form (Kusamo et al., unpublished), it is possible that conversion the dehydrogenase to an oxidase plays some as-yet identified role in the milk secretion process. In addition to its well-established role in purine metabolism, the dehydrogenase:oxidase conversion has been postulated to play an important role in the pathology of post-ischemic reperfusion injury in humans, involving the generation of reactive oxygen species superoxide and peroxide [76,77], and possibly hydroxyl radical.

Human diseases associated with genetic dysfunction of xanthine oxidoreductase are termed xanthinuria, because of excretion of xanthine in urine [94]. Patients also often have low levels of uric acid (less than 1 mg/dl) in blood. While mammals other than primates cannot survive xanthinuria due to kidney damage resulting from xanthine stones in the urinary tract [93,95], human xanthinuria patients generally do not show severe symptoms [94]. There are three types of xanthinuria, designated I–III. Type I xanthinuria is due to a defect in the gene encoding xanthine oxidoreductase that renders the protein non-functional or unstable; Type II xanthinuria involves a double deficiency of xanthine oxidoreductase and the closely related aldehyde oxidase (see below) that is the result of a defect in the molybdopterin sulfurase gene, the product of which catalyzes sulfuration of the molybdenum centers of the two enzymes [96], which is essential for catalytic activity; Type III xanthinuria involves a triple deficiency of xanthine oxidoreductase, aldehyde oxidase and sulfite oxidase, due to a defect in the synthesis of the molybdopterin/pyranopterin cofactor common of all three enzymes. This extremely seriously condition involves a number of problems associated with the central nervous system, and except in very rare cases [148] leads to death within the first year. In uricoteric animals such as birds and reptiles, xanthine dehydrogenase is involved in the pathway for nitrogen secretion, in which several equivalents of ATP are utilized in IMP biosynthesis. The enzyme thus plays a role in the recovery of energy expended for *de novo* synthesis of purine [76]. Indeed, NADH produced by xanthine dehydrogenase is utilized as an energy source in some bacteria [97]. In fruit flies, xanthine dehydrogenase is transported from fat bodies or Malpighian tubules to the eye, where it is involved in the biosynthetic pathway leading to the eye pigment drosopterin [98]; genetic lesions in the xanthine dehydrogenase gene give rise to the well-studied *rosy* phenotype, so named because of the distinctive eye color of flies unable to make drosopterin.

Xanthine oxidoreductase inhibitors: Human xanthine oxidoreductase is the target of drugs for treatment of hyperuricemia and gout [99–101]. Inhibition at the molybdenum center is important from a therapeutic viewpoint, because many proteins containing flavin or iron–sulfur cofactors exist in the human body, and if they were also inhibited, there might be deleterious side effects. On the other hand, only four molybdenum-containing enzymes are known in humans (xanthine oxidoreductase, aldehyde oxidase and sulfite oxidase discussed above, plus the newly discovered mARC systems, see below). As described above, deficiency of these enzymes, except sulfite oxidase [94,102], does not cause severe symptoms. Further, the active site of sulfite oxidase is quite different from that of xanthine oxidoreductase, and cross-inhibition generally does not occur. As inhibitors of xanthine oxidoreductase that target the molybdenum center also inhibit formation of reactive oxygen species generated by the enzyme, they might also be effective in the treatment of other diseases related to reactive oxygen species, although no clinical treatment based on this principle presently exists. It should be noted, however, that from a metabolic point of view inhibition of xanthine oxidoreductase results in an increase of IMP synthesis via the hypoxanthine phosphoribosyl transferase-dependent salvage pathway; this leads to feedback inhibition of *de novo* IMP synthesis owing to the inhibition of phosphoribosylpyrophosphate (PRPP) synthetase and glutamine PRPP amidotransferase by IMP [100,101], which improves the effectiveness of the inhibitors for gout therapy.

Many anti-cancer drugs are purine analogues and can be metabolized by xanthine oxidoreductase, so combined administration of chemotherapeutic agent and enzyme inhibitor needs to be monitored carefully, as greater drug efficacy can lead

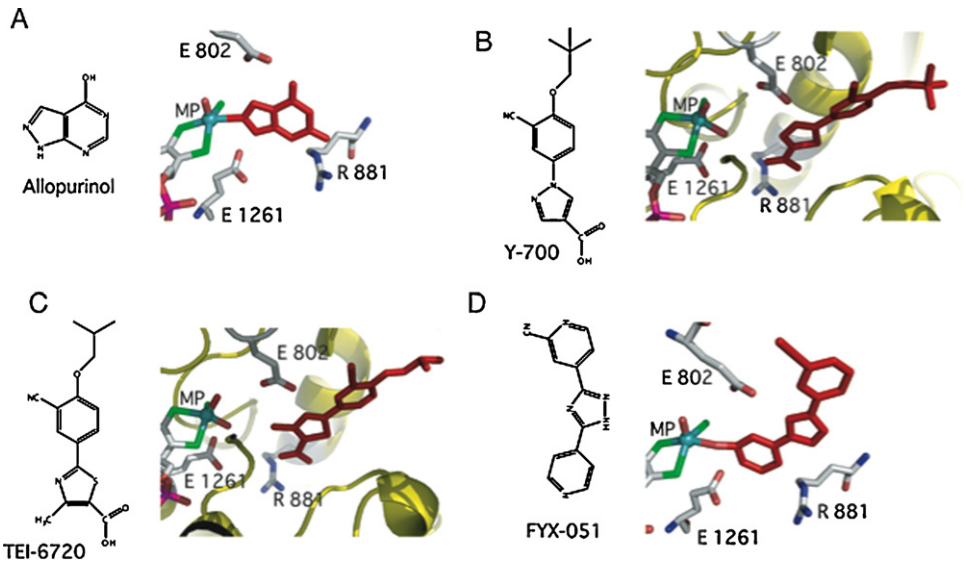

Fig. 10. Crystal structures of bovine milk xanthine oxidoreductase bound with potent inhibitors. A, alloxanthine; B, Y-700; C, TEI-6720; and D, FYX-051.

to greater toxicity [101]. Several potent inhibitors have been well characterized, including X-ray crystal structure analysis of the protein–inhibitor complex. Inhibitors can be classified into three types: mechanism-based, structure-based and hybrid types. Allopurinol (4-OH-pyrazolo[4,4-d]pyrimidine), a hypoxanthine isomer, was first synthesized by Robbins [103] and was introduced by Elion as a potent inhibitor of xanthine oxidoreductase more than 40 years ago [101]; it has been extensively prescribed for gout and hyperuricemia and is a generally well-tolerated drug, although minor side effects such as gastrointestinal irritation have been reported. Allopurinol, a mechanism-based inhibitor, is oxidized by xanthine oxidoreductase and the product alloxanthine (4,6-di-OH-pyrazolo[4,4d]pyrimidine) binds tightly to the reduced molybdenum center of the enzyme [65]; therefore, it is a kind of suicide inhibitor. The crystal structure of the alloxanthine-complexed form of bovine milk xanthine oxidoreductase has been determined at 2.1 Å resolution [104]. The features are very similar to those reported for bacterial xanthine dehydrogenase bound with allopurinol, determined at 3 Å resolution [66]. Clear electron density is observed between alloxanthine and the molybdenum atom. The N2 nitrogen replaces the equatorial hydroxyl ligand of the molybdenum, coordinating directly to the metal (Mo–N distance, 2.3 Å). Moreover, alloxanthine forms hydrogen bonds with Glu 802, Arg 880 and Glu 1261 of the enzyme, which are essential for the catalytic reaction [see Section 2.3]. Thus, it was supposed that the apical alloxanthine nitrogen atom replaces the catalytically labile Mo–OH ligand, with stabilizing hydrogen bonds to these three residues. This complex, however, decomposes slowly ($t_{1/2}$ = 300 min at 25 °C) accompanied with spontaneous reoxidation [65]. The non-purine analogs Febuxostat (TEI-6720; (2-[3-cyano-4-isobutoxyphenyl]-4-methyl-5-thiazolecarboxylic acid) [105] and Pyranostat (Y-700; 1-[3-cyano-4-(2,2-dimethylpropoxy)phenyl]-1H-pyrazole-4-carboxylic acid) [106] are structure-based inhibitors that have recently been developed. The crystal structures of the enzyme in complex with these compounds indicate that the inhibitors bind in the solvent access channel to the active site and have multiple interactions with various amino acid residues along the access channel (Fig. 10); consequently, they inhibit the enzyme activity with extreme low K_i values (*e.g.*, mixed-type inhibition with K_i 120 pM and K_i' 0.9 nM for TEI-6720) [105]. FYX-051 (4-[5-pyridin-4-yl-1H-[1,2,4]triazol-3-yl]pyridine-2-carbonitrile), a hybrid-type inhibitor, is a slow substrate which forms a covalent complex in the purine substrate channel. The electron density map at 1.9 Å resolution clearly shows that the Mo=S group found in the oxidized enzyme is protonated to Mo–SH (Mo–S distance, 2.4 Å) upon reduction of the molybdenum center [18]. The bridging electron density represents a bridging oxygen, derived from the Mo–OH group of the oxidized enzyme at the apex of the bent electron density, and the Mo–O and C2–O distances are 2.0 Å and 1.3 Å, respectively, with an Mo–O–C angle of 152°. The latter is a typical C–O distance for a hydroxylated six-membered ring. FYX-051 also has various interactions with amino acid residues in the substrate binding site and solvent access channel, being similar to Febuxostat in this respect. As FYX-051 has features of both mechanism-based inhibition and structure-based inhibition, it is expected to inhibit the enzyme strongly even in the absence of covalent bond formation [107].

Xanthine dehydrogenase to xanthine oxidase conversion: In the course of catalysis, reducing equivalents introduced into the enzyme at the molybdenum center from the purine substrate are transferred rapidly via the two [2Fe–2S] centers to the FAD cofactor, where the reduction of NAD^+ or molecular oxygen occurs [see Section 2.4]. Thus, conversion from xanthine dehydrogenase to xanthine oxidase has mainly to do with the conformation of the FAD domain, although the trigger sites are located some distance from the FAD itself [92]. In the xanthine dehydrogenase conformation the half-potential of the $FAD/FADH^\bullet$ couple is significantly higher than that for the $FADH^\bullet/FADH_2$ couple, indicating that the flavin semiquinone is thermodynamically stabilized [108–111]. The principal product of flavin with O_2 substrate is hydroquinone, with a lower second-order rate constant for $FADH^\bullet$ to give O_2^- as the product, instead of H_2O_2 in the case of $FADH_2$, which has a higher rate constant [76,77]. This accounts, at least in part, for the lower reactivity of FAD of xanthine dehydrogenase with O_2 with production of more O_2^- as compared with xanthine oxidase. On the other hand, binding of NAD^+ lowers the reduction potential of the FAD, facilitating electron transfer from the reduced $FADH_2$ to NAD^+ [76,77]. In the oxidase configuration, the lower affinity for NAD^+ and lower stability of the semiquinone as compared with the dehydrogenase configuration account for the higher reactivity toward O_2 [76,77].

Based on the three-dimensional folding of the FAD domain, the protein belongs to the so-called PCMH (*p*-cresol methylhydroxylase) family of flavoproteins. The FAD binds in an extended conformation in a deep cleft and the *si*-face of the isoalloxazine

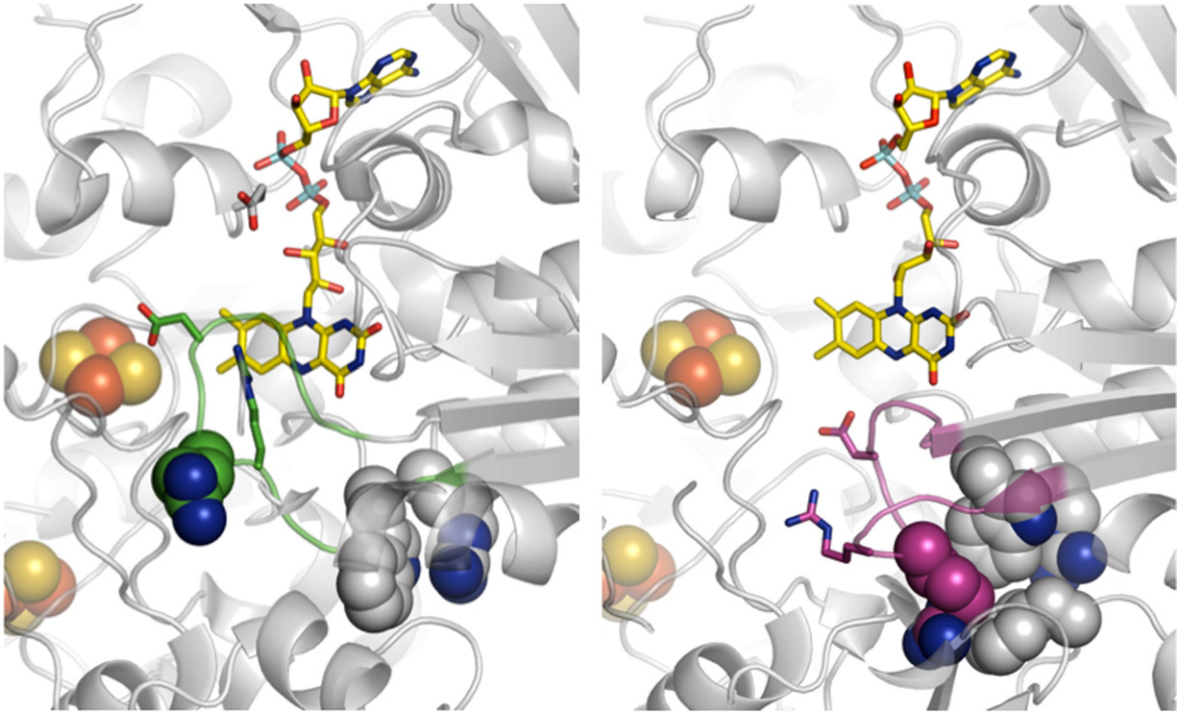

Fig. 11. Crystal structures around FAD cofactor of xanthine dehydrogenase and xanthine oxidase forms of bovine milk xanthine oxidoreductase. FAD is shown in yellow color stick model, while iron–sulfur centers and unique amino acid cluster are shown in space fill model. (left) Xanthine dehydrogenase form, A-loop is shown in red–purple color with important residues (atom color) (right) xanthine oxidase form, A-loop is shown in green color with important residues (atom color).

ring is easily accessible to solvent. This also allows the nicotinamide ring of NAD^+ align parallel to the isoalloxazine ring. The *re*-side of the FAD is sterically occluded and is not solvent accessible. One of these amino acids, Phe 337 in the bovine milk enzyme, is conserved in all known xanthine oxidoreductase sequences; its benzene ring forms a π–π stacking interaction with the pyrimidine subnucleus of the isoalloxazine ring. The phenylalanine, however, is replaced by non-aromatic residues in several obligate oxidases, *e.g.*, leucine in most mammalian aldehyde oxidases [112].

The difference between the crystal structures of the dehydrogenase and oxidase forms of the bovine enzyme is associated with a change in the location of a polypeptide loop from Gln 423 to Lys 433 [13] on the *si* side of the isoalloxazine ring of the FAD. In the dehydrogenase configuration (Fig. 11, left), the side chain of Asp 429 is close to C_6 of the flavin ring. With no positively charged residue nearby, Asp 429 provides a strong negatively charged environment for the FAD. The electrostatic potential is dramatically changed once the enzyme adopts its xanthine oxidase conformation, in which the conformation of this loop is quite different. Asp 429 moves away from the flavin ring and the guanidinium group of Arg 426 replaces it, approaching to within 6.3 Å of the isoalloxazine ring (Fig. 11, right). This reversal of the electrostatic potential surrounding the redox-active part of the FAD accounts for the changes in biochemical and biophysical properties of the FAD that are associated with conversion of the dehydrogenase to the oxidase. The dislocation of the loop also blocks NAD^+ from approaching the FAD, thereby obstructing NAD^+ binding in the oxidase configuration. Another important structural difference is found in a unique cluster of four amino acids, Arg 335, Trp 336, Arg 427 and Phe 549 (bovine enzyme), which are held together by π-cation interactions in the dehydrogenase configuration (Fig. 11, left) that are disrupted in the oxidase configuration [113].

The sites of proteolysis and formation of disulfide bonds that accompany the irreversible and reversible conversion of the dehydrogenase to the oxidase configuration, respectively, have been identified in rat xanthine oxidoreductase [114], and are most likely the same in the bovine enzyme because of the highly similar primary and three-dimensional structures [77,92]. The residue numbers given here are those for the bovine enzyme. The modification sites related to the conversion are in the linker peptide between the FAD and molybdenum domains (residues 532–589), the within the FAD domain (residues 226–531) and within the molybdenum domain (residues 590–1316). Proteolysis involves cleavage after Lys 551 and Lys 569 by trypsin and pancreatin, respectively, and disulfide bridge formation between Cys 535 and Cys 992, although the C-terminal peptide, which is involved in the slow conversion, was suggested to assist the NAD^+ binding [114].

As the crystal structures of both the dehydrogenase and oxidase forms of the bovine enzyme have been have been determined [13], the functional changes can be correlated with the underlying three-dimensional structures. The long linker peptide connecting the FAD and molybdenum domains contains not only the primary proteolytic cleavage site, but also one of the cysteine residues involved in disulfide bond formation that is associated with the dehydrogenase-to-oxidase transition [92,114]. Therefore, it seems reasonable to assume major changes in the arrangement of amino acids in this stretch of polypeptide can acts as a trigger for the transformation. The R335/W336/R427/F549 π-cation cluster seems to be at the center of a relay system [113]. Tight interactions between these residues seem to be crucial for the stabilization of the xanthine dehydrogenase form of the enzyme. Proteolysis, leading to increased mobility of the linker peptide, or disulfide formation, induces a conformational change that breaks Phe 549 out of this ensemble [113]; mutation of Trp 336 has an equivalent effect [115]. During these conformational changes, the cluster appears to act not only as a transmitter of modification at the linker peptide, but also as a solvent gate. Disruption of the cluster is transmitted to the loop described above, whose reorientation drives the conversion from dehydrogenase to oxidase.

2.6. ABA3 and sulfuration of xanthine oxidoreductase and aldehyde oxidase

It has been known for more than 40 years that xanthine oxidase, aldehyde oxidase and other members of the xanthine oxidase family possess a specific sulfur atom that can be abstracted by cyanide treatment in the form of thiocyanate, which leads to inactivation of the respective enzyme [52]. It was not until the functional and desulfo forms of xanthine oxidoreductase were compared by XAS, however, that the nature of the sulfur as a Mo=S was established [116]. It was also known that, in contrast to xanthine oxidoreductase and aldehyde oxidase, sulfite oxidase was not susceptible to cyanide treatment, indicating a fundamental difference between the enzymes [117,118]. While it proved possible to reconstitute the desulfo xanthine oxidoreductase with sulfur *in vitro* by incubation with sulfide under strongly reducing conditions [119], little was understood about how this sulfur was incorporated into enzyme under physiological conditions.

The first clue as to how sulfur incorporation occurred came from characterization of the fruit fly *maroon-like* (*ma-l*) mutant. Due to the reduced ability to form the red eye pigment drosopterin, these mutant flies are characterized by a readily detected maroon-like eye color that is the result of lost xanthine oxidoreductase activity [120]. In addition to xanthine oxidoreductase, the activities of aldehyde oxidase [121] and pyridoxal oxidase [122] were pleiotropically lacking in *ma-l* mutants, attributable ultimately to the requirement of a terminal sulfur ligand of the molybdenum cofactor by these proteins. In contrast, sulfite oxidase was unaffected in *ma-l* flies and it was concluded sulfite oxidase did not require a terminal sulfur ligand [123]. As shown later by the biological *nit-1* reconstitution assay, which is based on the reconstitution of a cofactor-free apo-nitrate reductase by a cofactor-containing extract of any origin, *ma-l* flies possessed wildtype-levels of molybdenum cofactor, excluding the possibility of a mutation in molybdenum cofactor biosynthesis [124]. Instead, it was assumed that *ma-l* mutants had a lesion in post-translational sulfuration which was essential for the activity of xanthine oxidoreductase, aldehyde oxidase and pyridoxal oxidase, but not of sulfite oxidase. By reconstituting the activities of xanthine oxidoreductase, aldehyde oxidase and pyridoxal oxidase in extracts of *ma-l* flies by sulfide/dithionite treatment it was shown that the mutation indeed affected the incorporation of sulfur into the cofactor of these enzymes [125]. These findings demonstrated that the sulfuration and activation of xanthine oxidase family enzymes were genetically controlled.

A phenotype similar to *ma-l* mutant flies is exhibited by the *Aspergillus nidulans hxB* (hypoxanthine non-utilizer, gene B) mutant, which is unable to grow on hypoxanthine or nicotinate as sole nitrogen source due to the simultaneous loss of xanthine oxidoreductase and nicotinate hydroxylase activities [126,127]. In contrast to these enzymes, nitrate reductase is not affected in *hxB* mutants as its molybdenum center, like that of sulfite oxidase, does not require a terminal sulfur ligand. Thus, as with the fruit fly *ma-l* mutants, *A. nidulans hxB* mutants affect the enzymes of the xanthine oxidase family whereas enzymes of the sulfite oxidase family are unaffected. The *ma-l* locus in fruit fly and the *hxB* locus in *Aspergillus* proposed to encode proteins designated as "molybdenum cofactor sulfurases". Cloning and *in silico* analysis of the *ma-l* and *hxB* cDNAs revealed that eukaryotic molybdenum cofactor sulfurases consist of two domains, an NH_2-terminal domain with similarities to bacterial cysteine desulfurases and a C-terminal domain, whose function was unknown [128]. Interestingly, although the biosynthetic pathway for molybdopterin is highly conserved between pro- and eukaryotes, the sulfuration systems – XdhC and ABA3, respectively – have proven to be quite distinct (see below).

Mutations resulting in deficiencies in the molybdenum cofactor sulfurase gene have been described in cattle [95], humans [96,129,130], silkworm [131], tomato [132], tobacco [133], and *Arabidopsis thaliana* [134–138]. Although all these mutants are characterized by essentially identical biochemical phenotypes, *i.e.*, by reduced or abolished activities of xanthine oxidase family enzymes with activities of sulfite oxidase family enzymes left unaffected, the pathology is significantly different in animals and plants. As indicated above, molybdenum cofactor sulfurase deficiency in animals, in particular mammals, is referred to as xanthinuria type II, an autosomal-recessive disease primarily caused by the loss of xanthine oxidoreductase activity. Affected individuals are characterized by reduced levels of uric acid in serum and urine with concomitant accumulation of xanthine and hypoxanthine. In humans, xanthinuria type II only rarely leads to xanthine stones in the kidney, urinary tract infection and acute renal failure [139]. On the other hand, the genetic lesion results in early death in other mammals, such as cattle [95]. Symptoms that can be attributed to the loss of aldehyde oxidase activity have not been reported as yet and at present xanthinuria type II is distinguished from xanthinuria type I (the isolated deficiency of xanthine oxidoreductase due to a mutation in the structural gene) by means of the allopurinol loading test [140]. In contrast to animals, molybdenum cofactor sulfurase-deficiency in plants is due principally to impaired aldehyde oxidase activity, and mutants, *e.g.*, from tobacco [133], tomato [132] and *A. thaliana* [96,129,130] exhibit aberrant stomatal control, excessive water loss, a wilty phenotype, reduced seed dormancy, and reduced stress tolerance. All symptoms are caused by reduced levels of the plant hormone abscissic acid, which is synthesized by a specific aldehyde oxidase by oxidation of the abscissic acid precursor abscissic aldehyde [141].

Although cDNA encoding molybdenum cofactor sulfurases has been isolated from several organisms [96,95,131,142,143], detailed biochemical information is available only for the molybdenum cofactor sulfurase ABA3 from *A. thaliana*. ABA3 is a homodimeric protein consisting of two ~92 kDa monomers, each being subdivided into two domains [141]. The NH_2-terminal domain of ~56 kDa shares significant similarities to the bacterial cysteine desulfurases SufS, NifS, and IscS, which provide sulfur for a number of cellular processes such as iron–sulfur cluster biogenesis. Like the bacterial cysteine desulfurases, the NH_2-terminal domain of ABA3 possesses a pyridoxal-5′-phosphate cofactor, which is crucial for the activity of the protein in which sulfur is abstracted from L-cysteine [143,144]. The sulfur is transferred to a conserved cysteine residue of the protein (Cys 430) as a persulfide, which can easily be removed by reduction and transfer to other thiol groups. Recent experiments with the heterologously expressed NH_2- and C-terminal domains of ABA3 indeed suggest that the sulfur is only transiently bound to Cys 430 and is subsequently transferred to a second cysteine residue in the NH_2-terminal domain and finally to two surface-exposed cysteine residues in the C-terminal domain [Lehrke, M., Mendel, R.R., and Bittner, F., unpublished data]. Together with the finding that the 35 kDa C-terminal domain of ABA3 binds molybdenum cofactor in its sulfur-free as well as in its sulfurated form [145], these observations indicate that the C-terminal domain acts, minimally, to: (i) bind the desulfo form of the cofactor and (ii) insert the sulfur into the molybdenum coordination sphere of the ABA3-bound cofactor. It remains unclear whether ABA3 finally activates its target enzymes xanthine oxidoreductase and aldehyde oxidase by transferring only the sulfur, which is bound to the molybdenum cofactor of the C-terminal domain, or by transferring the entire sulfurated molybdenum cofactor to xanthine oxidoreductase and aldehyde oxidase. In the first case, the C-terminus would exclusively act as a scaffold for the assembly of a molybdenum–sulfur center, which releases the sulfur and passes it to the desulfo-molybdenum cofactor of xanthine oxidoreductase

and aldehyde oxidase. Afterwards, the ABA3-bound molybdenum cofactor would again be in the desulfo-form and could take another sulfur from the NH_2-terminal domain. In the second case, the reaction catalyzed by ABA3 would be an exchange reaction in which desulfo molybdenum cofactor of xanthine oxidoreductase and aldehyde oxidase is replaced by sulfurated molybdenum cofactor from the C-terminal domain. ABA3 would exchange the desulfo-molybdenum cofactor of its target enzymes, with the extracted desulfo cofactor regenerated with sulfur provided by the NH_2-terminal domain. Although at first appearing unlikely, the second alternative must be seriously considered since the ABA3-bound cofactor can be removed without disturbing the protein's integrity (*e.g.*, by anion exchange chromatography), and at the same time is tightly bound by cofactor-free ABA3 when provided exogenously [145]. This suggests that the cofactor is bound to the surface of the C-terminal domain of ABA3 rather than in a deeply buried binding pocket as is found in members of the xanthine oxidase family. In support of this, a cofactor-binding motif around a strictly conserved arginine residue (Arg 723 in *A. thaliana*, Arg776 in *Homo sapiens*) within a "FRXN" sequence has been identified by analysis of mutations in the molybdenum cofactor sulfurase gene in plants [145] and humans [130]. Although a crystal structure is still lacking, computational analysis indeed predicts this motif to be localized on the surface of the C-terminal domain of molybdenum cofactor sulfurases. Such binding mode would not only support sulfuration of the ABA3-bound cofactor but could also be a prerequisite for cofactor supply or exchange reactions as discussed in Section 2.6 above.

2.7. Molybdenum cofactor insertion

The manner in which the deeply buried molybdenum center of xanthine oxidase and related enzymes is incorporated into the apoprotein has been of continuing interest over the past decade. Very recently, Hall and Hille (unpublished) have identified a very highly conserved ~125 amino acid region of the crystallographically characterized bovine enzyme (Fig. 12, A–D), whose rotation into a new position opens a channel that might plausibly provide access to the binding site for the cofactor in the apoprotein (compare Fig. 12B with Fig. 12D). At the same time, this motion appears to create a structural motif that may be recognized by the insertion machinery of the cofactor. Upon energy-minimization, this putative "open" configuration is stabilized by specific interactions between the two hinge regions in the homo(apo)dimer, including a pair of electrostatic interactions between Glu 1092 of one subunit and Arg 1099 of the other, as well as a hydrogen bond between Thr 1095 of each subunit (Fig. 12E). In the "open" configuration, the two hinge domains swing together and close a large groove on the surface of the dimer, and assemble to form a single structural element that has a relatively flat, solvent-exposed surface from which two capping motifs protrude at either extreme (Fig. 12C, red). These regions together may constitute a recognition site for the ABA3/HMCS insertion machinery when in the "open" configuration. The cap motifs of the hinge region are extremely acidic, suggesting that the complementary portion of the insertion machinery is positively charged. Importantly, while the two new channels to the cofactor binding sites of the dimer lie on opposite sides of the now merged hinge domains, they lie on the same face of the overall dimer, an orientation that could allow the dimeric insertion machinery to insert the two molybdenum centers simultaneously into both subunits of the dimer.

The newly created channel (seen immediately to the lower right of the red hinge region in the righthand subunit of Fig. 12D) in each subunit lies on the opposite side of the cofactor binding site from the substrate access channel to the active site. The implication is that the molybdenum center must be inserted "molybdenum first", entering from what has conventionally been understood to be the back side of the protein structure. The pyranopterin ring portion of the mature molybdenum center enters next (its distal amino group lies close to, and possibly hydrogen bonds, one of the cysteine ligands to the nearer [Fe–2S] cluster in the adjacent domain of the protein [16]), followed last by the side chain phosphate of the cofactor. In the *Oligotropha carboxydovorans* CO dehydrogenase [149], another member of the xanthine oxidase family that possesses an elaborated cytosine dinucleotide form of the pyranopterin cofactor, the cytidine portion of the cofactor extends toward the protein surface sandwiched between the (now collapsed) walls of the putative cofactor access channel identified here [16]. The phosphate group of the molybdenum center, once inserted, appears to play an important role in triggering closure of the cofactor access channel, by means of an interaction with the positively charged amino terminus of the longer α helix of the hinge region.

In prokaryotic members of the xanthine oxidase family, there is a 19-residue insert in the cap motif of the hinge region that is absent in eukaryotic enzymes, and a second 20-residue insert elsewhere on the dimer surface near the hinge domain [146]. These inserts may also be involved in recruiting of the cofactor insertion machinery, and their absence in the eukaryotic enzymes suggests that the manner in which the insertion machinery interacts with apoprotein may differ in its structural details between prokaryotes and eukaryotes. The interested reader is referred to other contributions to this issue for a fuller description of cofactor biosynthesis and insertion in prokaryotes [147] and eukaryotes [148].

3. Aldehyde oxidase

3.1. Gene distribution in animals and higher plants

The vertebrate aldehyde oxidases are closely related to the xanthine oxidoreductases described above, sharing very similar overall protein architectures, overlapping substrate specificities and the requirement for a catalytically essential Mo=S group in the molybdenum coordination sphere. Given the difficulty in isolating the enzyme in quantity from liver, however, much less work has been done with aldehyde oxidase as compared to the xanthine-utilizing enzyme. Still, as discussed further below, it is widely considered that the overall mechanism of aldehyde oxidation proceeds essentially identically to that described above for xanthine oxidation, with base-assisted nucleophilic attack of a Mo–OH on the substrate carbonyl, with hydride transfer to the Mo=S to yield the two-electron reduction of the molybdenum center. Interestingly, the mammalian aldehyde-oxidizing enzymes are always found as the oxidase – there is no example of a eukaryotic aldehyde dehydrogenase utilizing NAD^+ as oxidizing substrate.

In mammals, the copy number for genes encoding aldehyde oxidases (AOX) and aldehyde oxidase homologs (AOH) is variable: humans have a single-copy *Aox1* gene and no *Aoh* genes, while most rodent genomes that have been examined possess one *Aox1* gene and three genes *Aoh1-3* encoding proteins that differ very modestly in amino acid sequence from one another and from AOX; the intron/exon structure of these genes is also highly conserved, reflecting the gene duplication events from which they arose [150]. Mammalian aldehyde oxidases oxidatively hydroxylate a variety of drugs, particularly aromatic heterocycles, but the physiological substrate(s) remain unknown. The enzyme has been ascribed a role in the conversion of retinaldehyde to retinoic acid [151], but this requires comment. Retinoic acid plays a critical role in limb development in vertebrates during embryogenesis, yet individuals with a genetic lesion in the molecular apparatus that sulfurates xanthine oxidase and the aldehyde oxidases have relatively minor clinical symptoms and no evident developmental abnormalities [96,129,130]. A mouse knockout for the *Aoh2* gene has been generated [152], and the individuals are seen to have developed normally,

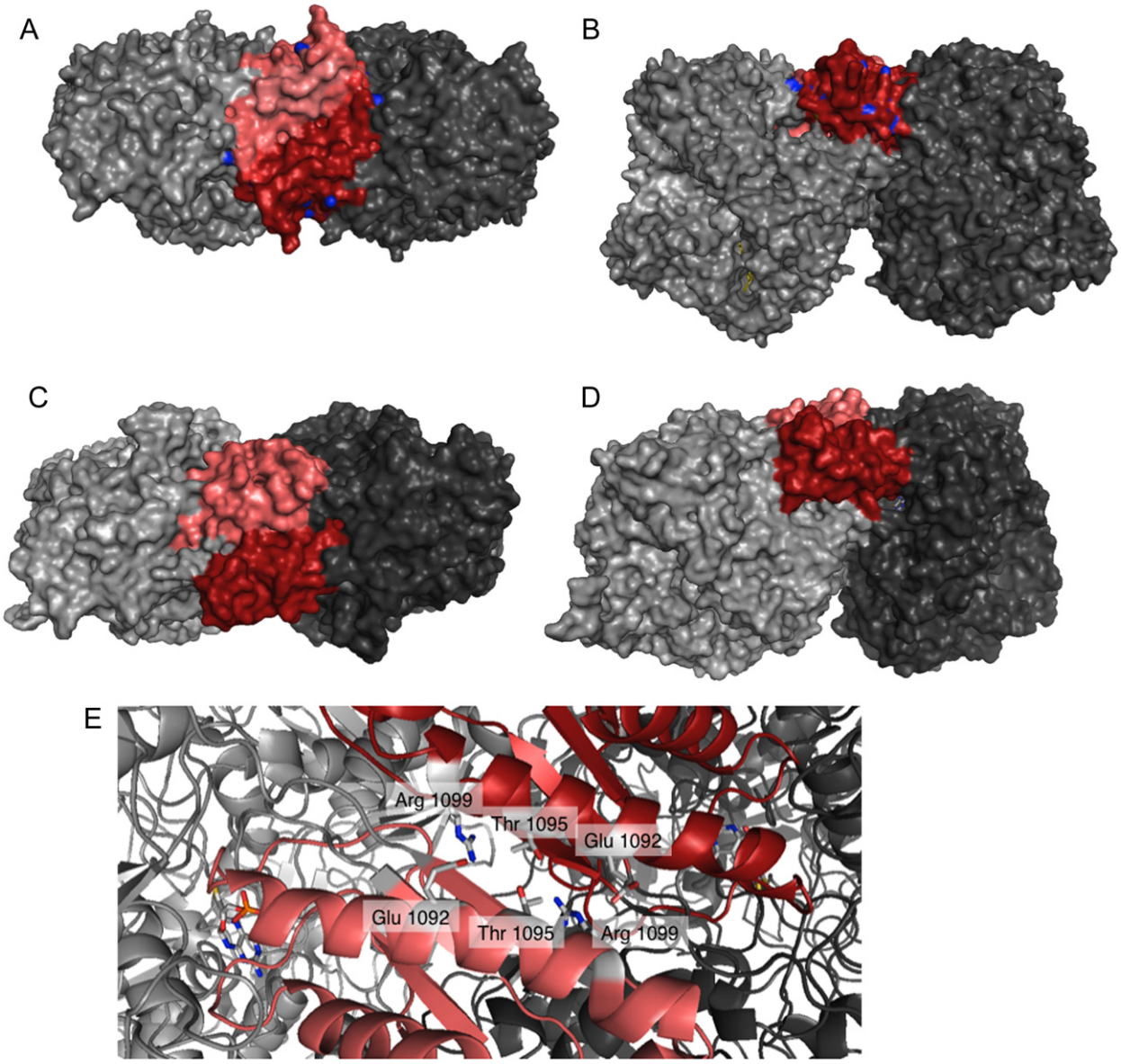

Fig. 12. Putative hinge regions involved in providing access to the molybdenum cofactor binding site of apo xanthine oxidase from bovine milk. A, a surface representation of the dimeric holoenzyme with subunits shaded light and dark, respectively, with the putative hinge regions in red. The perspective is along to the non-crystallographic C_2 axis of symmetry for the molecule. B, The holoenzyme viewed from the side. C, A surface representation of the energy-minimized "open" configuration of the apoprotein, viewed along the non-crystallographic C_2 axis of symmetry. D, The energy-minimized "open" structure from the side, illustrating the large channel (seen to the lower right of the red hinge region in the righthand subunit of Panel D) opened after the hinge regions have been rotated out of position, as described in the text. The position of the pterin cofactor is indicated in the subunit on the right. E, a close-up of the hinge regions in the putative "open" configuration, viewed along the non-crystallographic C_2 axis of symmetry. The spontaneously formed electrostatic interactions between Glu 1092 of one subunit and Arg 1099 of the other, the hydrogen-bonding interaction between Thr 1095 of the two subunits that could stabilize the putative "open" structure.

and even are fertile. On the other hand, retinoid metabolism in specific tissues (most notably the skin) is perturbed and retinoid-dependent genes are generally down-regulated, suggesting that AOH2 is involved in the local biosynthesis and biodistribution of retinoic acid in the affected tissues. Other unrelated retinaldehyde dehydrogenases are thought to be involved in the ontologically critical biosynthesis of retinoic acid [150].

There are two to four genes encoding aldehyde oxidases in higher plants [150], encoding enzymes that catalyze the final steps in the biosynthesis of the important plant hormones abscissic acid and indole-3-acetic acid. In each case, the reaction catalyzed represents the oxidative hydroxylation of the respective aldehyde to the bioactive carboxylic acid. In *A. thaliana* there are four genes, AOX1–4 [153,154], with AOX3 specifically involved in abscissic acid biosynthesis in leaves (but not seeds) [153,155]. In *Pisum sativum*, there are three genes encoding aldehyde oxidases, *Psaox1-3*, the last appearing to encode a stress-specific abscissic aldehyde oxidase [156]. None of the plant enzymes have been studied in great detail at a biochemical level, but by analogy to other enzymes of this family considerable overlap in substrate specificity among the plant aldehyde oxidases is to be expected. It is likely that the specific physiological roles of the gene products is due more to the manner in which gene expression is regulated in different plant tissues under different physiological conditions rather than to the intrinsic substrate specificity of the proteins encoded.

3.2. Protein structure and reaction mechanism

Although the first X-ray crystal structure of a member of the xanthine oxidase family to be obtained was that of the alde-

hyde:ferredoxin oxidoreductase from *D. gigas* [14], no crystal structure has been reported for a eukaryotic aldehyde oxidase. Since the eukaryotic aldehyde oxidases have much stronger sequence homology to the eukaryotic xanthine oxidoreductases than to the bacterial aldehyde-oxidizing enzyme (not least because the latter lacks an FAD-containing domain), the better starting point for understanding the active site structure of the aldehyde oxidases is the structure of the eukaryotic xanthine-utilizing enzyme. A comparison of the amino acid sequence of bovine, murine and human aldehyde oxidase genes with the bovine, human and mouse xanthine oxidoreductases allows some comparisons [6,152]. Referring to Fig. 4, the following amino acid residues are conserved between the mammalian xanthine- and aldehyde-utilizing enzymes: Gln 767, Phe 914 (that which stacks flat rather than side-on against bound substrate) and Glu 1261. Glu 802 of xanthine oxidase is a valine in the aldehyde oxidases (except in murine AOH1, where it is Ala) and Phe 1009 of xanthine oxidase is conserved in murine AOH1 and 3, but is a Leu, Ile or Val in the other four aldehyde oxidases. Finally, Arg 880 in xanthine oxidase is a Met in the proper aldehyde oxidases, or Phe/Tyr in the murine AOH forms. Given the specific catalytic roles in xanthine hydroxylation that have been proposed for Glu 802 [64] and Arg 880 [63], their lack of conservation in the aldehyde oxidases is to be expected.

Absent evidence to the contrary, and given the strict conservation of the glutamate residue thought to function as a general base, the reaction mechanism for the aldehyde oxidases is considered to be analogous to that described above for other members of this enzyme family, with base-assisted proton abstraction from the equatorial Mo–OH group initiating catalysis [39]. This is followed by nucleophilic attack on the carbonyl carbon of substrate with concomitant hydride transfer to the Mo=S group, through a tetrahedral transition state [157] in which the C–O bond of product is ~90% formed and the C–H bond of substrate ~80% broken in the transition state. Although the reaction is thought to involve nucleophilic attack on the highly activated carbonyl carbon and proceed through the same type of $LMo^{IV}O(SH)(OR)$ intermediate as seen with xanthine oxidase, no EPR signal equivalent to the "very rapid"; EPR signal seen with xanthine oxidase has been seen with aldehyde oxidase [158]. Human aldehyde oxidase oxidizes a spectrum of aromatic heterocycles in addition to aldehydes, as mentioned above, and many of these are therapeutically important – a DFT approach to understanding reactivity of the enzyme, in the context of a reaction initiated by nucleophilic attack on substrate, has successfully accounted for the experimentally observed regioselectivity of substrate hydroxylation for a number of aromatic heterocycles [159]. Recently, human aldehyde oxidase has been cloned and heterologously expressed in *E. coli*, and while expression levels were modest sufficient protein was obtainable to undertake steady-state kinetic studies [160]. Enzyme activity on a series of substituted quinazoline substrates analogous to that used previously with xanthine oxidase [41], gave the same general trend in reactivity (with the notable exception of the nitro derivative, which was found not to be an effective substrate for aldehyde oxidase).

4. Sulfite oxidase

4.1. Introduction to structures of plant and animal enzymes

The eukaryotic sulfite oxidases and other members of this family of molybdenum enzymes differ fundamentally from the xanthine- and aldehyde-utilizing enzymes described above in two regards: (1) their molybdenum centers possess two Mo=O groups and a cysteinyl ligand to the metal, $LMo^{VI}O_2$(S-Cys); and (2) the chemistry catalyzed is a simpler oxygen atom transfer reaction rather than a carbon center hydroxylation involving cleavage of a C–H bond. The X-ray crystal structures of sulfite oxidase from both a vertebrate (chicken) [161] and a plant (*A. thaliana*) [162] have been determined. Considering first the chicken enzyme (Fig. 11), each subunit of the homodimer consists of an N-terminal heme-containing domain with strong sequence and structural homologies to vertebrate cytochromes b_5, followed by a 12–15 residue long tether connecting the heme domain to the molybdenum-containing domain, which has a mixed α/β fold unique to this family of proteins, and finally a C-terminal domain that constitutes the dimer interface and possesses a β-sandwich fold typical of the C2 subtype of the immunoglobin superfamily of proteins (but lacks a disulfide bond that is an otherwise conserved structural feature of these proteins). As in the xanthine oxidase family of molybdenum enzymes, the redox-active centers of one subunit are well-separated from those of the other, some 38 Å at closest approach (molybdenum-to-molybdenum). In the crystal structure, the two heme domains of the dimer do not occupy the same orientation relative to their respective molybdenum subunits, and the hemes themselves are both >30 Å from their respective molybdenum centers – clearly domain motions are critical to electron transfer between molybdenum and heme within each subunit (see below).

By contrast to all vertebrate sulfite oxidases, the *A. thaliana* enzyme lacks a heme domain [163], although the remainder of the protein closely resembles the corresponding parts of the chicken enzyme [162], as shown in Fig. 13. The structure of the molybdenum-binding portion of the protein appears to represent an evolutionarily ancient motif that has remained highly conserved despite sometimes low sequence identity among proteins [164]. The fact that the *A. thaliana* sulfite oxidase possesses no redox-active sites other than the molybdenum center has made it possible to examine the molybdenum center of the enzyme spectroscopically without complications arising from more strongly absorbing chromophores [165]. The absorption spectrum of the oxidized enzyme has absorption bands at 480 and 360 nm, both of which exhibit positive ellipticity in the circular dichroism spectrum. Both bands bleach upon reduction of the enzyme, with a single weak shoulder at 400 nm. These spectral features corroborate those previously seen for the molybdenum-containing proteolytic fragment of chicken sulfite oxidase [166].

The active site of chicken sulfite oxidase (in its reduced form) is shown in Fig. 12A. In addition to an $LMo^{IV}O(OH)(S\text{-}Cys^{185})$ molybdenum center (with an elongated equatorial Mo–O bond interpreted as reflecting at least a single protonation to Mo–OH), a cluster of highly conserved residues consisting of Arg 138, Arg 190, Trp 204, Tyr 322 and Arg 450 surrounds a bound product sulfate molecule and clearly defines the substrate binding site. The sulfate lies near the equatorial oxygen of the molybdenum coordination sphere. The corresponding active site residues of the (oxidized) plant enzyme are Arg 51, Arg 103, Trp 117, Tyr 241 and Arg 374 (Fig. 12B). Interestingly, with no sulfate in the structure of the (oxidized) plant protein [58], Arg 374 is found in a substantially different configuration than the corresponding Arg 450 of the chicken enzyme, facing away from the substrate binding cavity rather than into it. From a comparison of the two structures, it appears that Arg 374/450 swings into place only when the substrate binding site is occupied. Subsequent crystallographic studies of the recombinant chicken enzyme in the absence of substrate have demonstrated that Arg 450 does indeed swing away form the substrate binding site in the absence of bound sulfate [167]. In the absence of sulfate, chloride occupies the binding site, interacting with Arg 190 and Trp 204. Unexpectedly, in the R138Q mutant (equivalent to the R160Q variant of the human protein identified clinically) Arg 450 faces into the substrate binding cavity, even in the absence of sulfate. As discussed further below, this appears to represent a "blocked" form of the enzyme.

A C207S mutant of the rat enzyme has been prepared, in which the Cys coordinating the molybdenum is replaced by a Ser. The

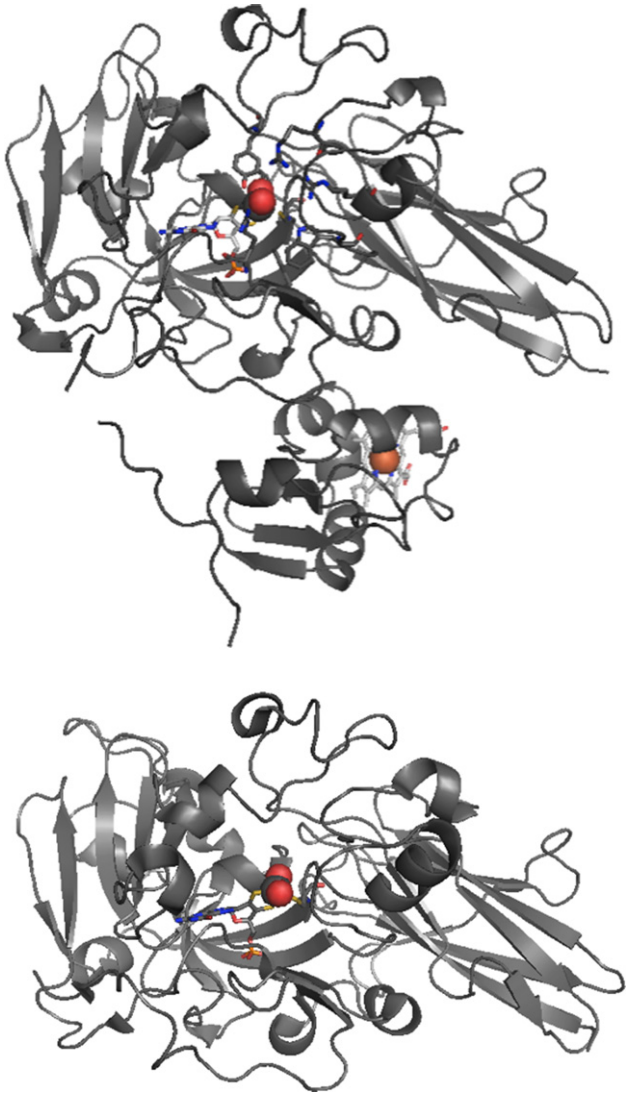

Fig. 13. Structures of the sulfite oxidase from chicken (top) and *A. thaliana* (bottom).

mutant exhibits a perturbed UV–vis absorption spectrum and a 2000-fold reduction in specific activity [168]. An examination of the mutant by XAS has concluded that the oxidized molybdenum center of the mutant protein possesses an $LMo^{VI}O_3$ core, and that Ser 207 in the mutant does not coordinate the metal [169]. Subsequently [170], it has been shown that potentiometric titration of the C207S mutant yields a reduced center with a single Mo=O group as determined by XAS, with the serine now presumably coordinated to the metal to give a $LMo^{IV}O(OH)$(O-Ser) species. The Mo–OSer bond appears to persist in the Mo(V) valence state at pH 6.0, which has an EPR signal with $g_{1,2,3}$ of 1.9789, 1.9654, 1.9545, significantly shifted from the values seen with wild-type enzyme ($g_{1,2,3}$ = 2.0037, 1.9720, 1.9658; [171]). Proton coupling is evident, but much weaker in the EPR signal of C207S mutant than is the case with wild-type enzyme [170]. More recently, Cys 185 of the chicken enzyme (equivalent to Cys 207 of the human enzyme) has been mutated to both Ser and Ala, and the variants comprehensively examined by X-ray crystallography and XAS [172]. The $LMo^{VI}O_3$ core is confirmed in the oxidized centers of both mutants, and neither could be reduced by sulfite to any appreciable degree. Interestingly, in the C185S mutant (but not the C185A mutant) Tyr 332 and the 31-residue loop on which it resides (residues 310–340) are disordered in the X-ray crystal structure, except for a short stretch that is found in a different configuration than seen in the wild-type enzyme. Clearly, there is some rearrangement in the vicinity of the active site upon mutation of Cys 207 to Ser. The interested reader is referred to another contribution to this issue for a more detailed discussion of the role of Cys in dictating the detailed electronic structure and reactivity of the active site of sulfite-oxidizing enzymes [173].

The molybdenum center of sulfite oxidase lies considerably closer to the protein surface than does that of xanthine oxidase, and the process of cofactor insertion appears to be more straightforward. Using a heterologously expressed apo form of the human enzyme, an *in vitro* system consisting of an isolatable intermediate in the pyranopterin biosynthetic pathway (termed "Precursor Z"), the sulfur-charged MoaDE MPT synthase from *E. coli* and molybdate is sufficient to reconstitute sulfite-oxidizing activity in the apoenzyme [174]. The data indicate that MPT synthase synthesizes MPT, and stabilizes it against air reoxidation. Molybdate is apparently not incorporated into the cofactor until after transfer of MPT to the apo sulfite oxidase. Neither MogA and MoeA, two gene products in *E. coli* that have long been thought to play a role in molybdenum insertion into the maturing cofactor, nor their eukaryotic homolog gephyrin are required in this *in vitro* system, possibly because of the relatively high molybdate concentrations utilized. It remains likely that these auxiliary proteins are essential for efficient cofactor insertion into apo sulfite oxidase at physiological concentrations of molybdate. The interested reader is again referred to other contributions to this issue for a more detailed discussion cofactor biosynthesis, maturation and insertion in prokaryotes [147] and eukaryotes [148].

4.2. The reductive half-reaction

Using a density functional approach, Hall and co-workers [175,176] have provided considerable insight into the reactivity toward oxygen atom transfer of $LMoO_2$ clusters of the type found in the active site of sulfite oxidase. The key element is the interaction between the lone pair of a suitable oxygen atom acceptor (a phosphine was used in the computational work) a π^* orbital of one of the two Mo=O groups (this is the equatorial Mo=O in the enzymes, which is oriented directly at the substrate binding pocket in the protein structure). With phosphine as acceptor in the computational study, P–O bond formation results in loss of the π interaction between the molybdenum and oxygen that is under attack, leading to formal two-electron reduction of the molybdenum. The two Mo=O groups of the oxidized complex compete for π ligation with the same set of molybdenum d orbitals, and the loss of the second Mo=O group in the course of the reaction allows the first to interact more strongly with the molybdenum – an interaction that involves one σ and two π interactions in a formal triple bond. This recoups some of the enthalpic cost of cleaving a strong metal–oxo bond, and labilizes the oxo group in what has been referred to as the "spectator oxo" effect [177].

Sulfite oxidase has been proposed to function in a similar fashion to that described above for the MoO_2 model compounds [178], a conclusion supported by a computational study of the enzyme's molybdenum center in which the reactivity of the equatorial oxygen of the molybdenum coordination sphere is specifically activated for oxygen atom transfer [179]. That the enzyme likely reacts in this way is reflected in its reactivity toward dimethylsulfite, a substrate analog in which the oxyanion groups of substrate have been blocked by methylation, leaving only the sulfite lone pair to participate in the reaction. In a rapid-reaction kinetic analysis of both sulfite and dimethylsulfite, the dependence of k_{obs} on [substrate] in both cases is hyperbolic, and while the K_d for substrate increases over 300-fold upon methylation (to 11 mM from 33 μM), the limiting rate of reduction at saturating concentrations of substrate is essentially unchanged (194 s^{-1} for sulfite, 170 s^{-1}

for dimethylsulfite) [180]. With control experiments undertaken to ensure that reactivity of dimethylsulfite was not due to slow hydrolysis to sulfite in aqueous solution, the following conclusions can be drawn: the oxyanion groups of sulfite contribute some 3 kcal/mol toward substrate binding, but are not the only forces that contribute to enzyme affinity for substrate (since k_{obs} shows a hyperbolic dependence on [dimethylsulfite]); once the binding site is saturated at sufficiently high substrate concentration, the reaction proceeds at the same rate with dimethylsulfite as with sulfite, meaning that the oxyanion groups are not involved in accelerating the rate of the chemical step of the reaction by, for example, directly coordinating to the molybdenum. Thus, despite the fact that direct oxygen atom transfer has not been demonstrated in the literature this mechanism is now generally accepted.

Reaction of the vertebrate sulfite oxidases with sulfite results in the two-electron reduction of the enzyme, and although the enzyme is not fully reduced (which requires three reducing equivalents) the reaction cannot proceed further as electrons are introduced in pairs in the oxidation of sulfite the molybdenum center. Reoxidation of the enzyme involves transfer of the two catalytically introduced electrons individually from the molybdenum center to the heme site of the enzyme, followed by reaction with cytochrome *c* at the heme site to reoxidize the sulfite oxidase. This reaction is consistent with the known subcellular localization in the intermembrane space of the mitochondrion, with reducing equivalents from sulfite thus entering the respiratory chain. A comparison of the pH dependence of both the reductive and oxidative half-reactions of the catalytic sequence indicates that under most conditions the reductive half-reaction (*i.e.*, the reaction of anaerobic, oxidized enzyme with sulfite) is predominantly rate-limiting, but that particularly at low pH the oxidative half-reaction (the reaction of reduced enzyme with cytochrome *c*) becomes partially rate-limiting [181]. In this study, k_{red}, the limiting rate of reduction at high [sulfite], was essentially pH-independent at 200 s^{-1}, while k_{red}/K_d (reflecting the bimolecular reaction of free substrate with free enzyme in the low [sulfite] regime) exhibited a sigmoidal pH dependence with a pK_a of 9.3, reflecting the ionization of a functional group that must be protonated for the reaction to proceed; this pK_a was tentatively assigned to Tyr 322 in the active site.

Subsequently, the steady-state and rapid-reaction kinetic behavior of human sulfite oxidase, both wild-type enzyme and a Y343F mutant, has been examined (Tyr 343 in the human enzyme corresponding to Tyr 322 in the chicken enzyme) [182]. Both the holoenzyme form and the molybdenum fragment alone were examined. The behavior of the wild-type holoenzyme enzyme closely mimics that previously seen for the chicken enzyme, as expected. The effects of the mutation in the holoenzyme can be summarized as follows: (1) both k_{cat} and k_{cat}/K_m in steady-state analysis are only modestly affected, the principal effect being shifts of ~1 pH unit in one limb of the bell-shaped pH profile – the maximum values for the two kinetic parameters are essentially unchanged at 25 s^{-1} and 4.5 × 10^6 M^{-1} s^{-1}, respectively; (2) the pH profile for k_{red} from rapid reaction studies following enzyme reduction by reduction of the heme is independent of pH at ~80 s^{-1} for the wild-type holoenzyme, but with the mutant is base-catalyzed, increasing from 5 s^{-1} at low pH to a maximum value above 60 s^{-1} above pH 9.5 with an apparent pK_a > 10; and (3) k_{red}/K_m is acid-catalyzed for both wild-type and mutant holoenzyme, both with a pK_a of 7.7 meaning that the ionization evident in the pH profile for wild-type enzyme cannot be due to Tyr 343 (or Tyr 322 in the chicken enzyme). With the molybdenum fragments alone, there is only a modest effect of the mutation on k_{red} (both ~2000 s^{-1} at pH 7) but K_d increases by approximately an order of magnitude (from 186 μM to 1.6 mM). The faster rate constants seen with the fragment as compared to the holoenzyme has been attributed to extremely rapid formation of a Mo^{IV}• sulfate giving rise to the spectral change being followed in the experiment, with subsequent electron transfer on to the heme being rate-limited by sulfate release in the case of the holoenzyme [182]. On the basis of this interpretation, Tyr 343 appears to contribute to substrate binding and also to facilitate product dissociation so that subsequent electron transfer out of the molybdenum center can occur. In both cases the amount of free energy involved is approximately 1.5 kcal/mol.

A clinically identified R160Q variant of human sulfite oxidase has also been recombinantly expressed and examined [183]. The mutation results in a decrease in k_{cat} from 16 s^{-1} to 2.4 s^{-1}, and a significant increase in K_m from 17 μM to 1.7 mM; the overall effect on k_{cat}/K_m is three orders of magnitude. Although K_m is not a proper thermodynamic parameter (expressed in terms of microscopic rate constants for any specific mechanism, it necessarily contains terms from multiple steps of the catalytic sequence, including some from the oxidative as well as the reductive half-reaction [184]), it is evident that substrate affinity is seriously compromised in the mutant (consistent with the known position of Arg 160 in the substrate binding site). Interestingly, as discussed further below, the predominant effect of the mutation is actually not on the reductive half-reaction of the catalytic cycle but on the rate constant for electron transfer from the molybdenum center to the heme, prior to electron transfer on to cytochrome *c*. It is worth noting that the corresponding Arg 55 in the closely related sulfite dehydrogenase from *Starkeya novella* has also been mutated to Met with comparable results to those seen with the chicken enzyme: the effect on the limiting rate constant for enzyme reduction at high [sulfite] is modest, but K_d increases three orders of magnitude [185].

4.3. Intramolecular electron transfer in chicken and human sulfite oxidase

Intramolecular electron transfer within the chicken and human sulfite oxidases has been extensively studied by Enemark, Tollin and co-workers over the past 10 years, using a deazariboflavin-based photolytic method to rapidly introduce reducing equivalents and follow subsequent intramolecular electron transfer spectrophotometrically [186]. Under most conditions, rate constants for electron equilibration between the molybdenum and heme (in the one-electron reduced enzyme) are on the order of 2000 s^{-1}, although at high pH and in the presence of anions such as sulfate the rate constant fall to as low as 35 s^{-1}. Given the known reduction potentials for the Mo(VI/V) and heme (III/II) couples, the forward and reverse rate constants can be deconvoluted [187], it being determined that the rate constant for Mo → Fe electron transfer is pH-independent at 700 s^{-1} while that for Fe → Mo electron transfer decreases approximately monotonically from 600 s^{-1} at pH 8.5 to 140 s^{-1} at pH 7 [187]. Qualitatively consistent with the notion that extensive heme domain motion is required for intramolecular electron transfer, it is observed that increasing solvent viscosity from 1.0 to 2.0 cP reduces the rate constant for intramolecular electron equilibration by a factor of two [188], although the small magnitude of the effect precludes a more quantitative treatment. Similarly, electron transfer is compromised upon reducing the length of the tether connecting the heme- and molybdenum-containing portions of human sulfite oxidase [189]. Reducing the length of the 14-aa tether sequence to nine residues reduces the rate constant for electron equilibration from ~450 s^{-1} at pH 7.0 to 6 s^{-1} (more modest deletions resulting in intermediate effects). A pulsed electron-electron double resonance (ELDOR) study examining the Mo(V)–Fe(III) distance in Ti^{III}• citrate-reduced chicken sulfite oxidase found (pumping the Mo(V) signal and observing the Fe^{III} heme) no evidence of dipole modulation, suggesting that in the frozen sample there is a broad distribution of Mo–Fe distances that implies conformational flexibility [190].

The effect of several point mutations on intramolecular electron transfer has also been investigated, for the most part restricted to studies with the human enzyme. Mutation of Tyr 343 to Phe, discussed above with regard to the effect on catalysis, reduces the observed rate constant for electron equilibration from 411 s^{-1} to 46 s^{-1} at pH 6.0, the effect being approximately the same for electron transfer in both the forward and reverse direction (the observed kinetics being consistently observed to be four- to five-fold slower in the human relative to the chicken enzyme) [191]. The effect of the mutation on electron transfer is likely to be an intrinsic one, and not an indirect one related to, *e.g.*, product release. Electron equilibration within the R160Q mutant discussed above is affected to an even greater degree, being reduced by a factor of almost 1000 from that seen in wild-type enzyme, from 411 s^{-1} to 0.64 s^{-1}; electron transfer from molybdenum to heme in this case is entirely rate-limiting for catalysis [192]. An R160K mutation that preserves the positive charge at position 160 exhibits only a four-fold reduction in the rate constant for electron equilibration, a result taken to suggest that the positive charge at position 160 plays a role in orienting the heme domain appropriately for effective electron transfer [192]. Other mutations identified on the basis of clinical manifestations of individuals with variants of sulfite oxidase are G473D and A208D, both located near the substrate binding site for the enzyme (Ala 208 is adjacent to Cys 207 that coordinates the active site molybdenum in the human enzyme). Both mutations decrease the rate constant for electron equilibration within one-electron reduced enzyme by a factor in excess of 1000 (to ~0.2 s^{-1} for G473D and 0.1 s^{-1} for A208D), making intramolecular electron transfer again entirely rate-limiting to catalysis [193]. The fact that a G473A mutant exhibits only modestly slower electron transfer than wild-type suggests that the principal effect in the G473D mutant is to the negative charge introduced by the mutation, although it is unclear whether this is due to an electrostatically compromised interaction with the heme domain, as thought to be the case with the Arg 160 mutants, or to the fact that the G473D mutant is simply conformationally compromised (as evidenced by a significantly perturbed CD signature in the near-UV and by its failure to dimerize).

In addition to the above studies directly probing electron transfer within sulfite oxidase, the enzyme's electrochemical properties have been examined by protein film voltammetry. Chicken sulfite oxidase immobilized on a pyrolytic graphite edge electrode yielded a noncatalytic wave at +90 mV (vs. SHE) in a cyclic voltammogram, and addition of 1 mM sulfite established a catalytic wave at the same potential [194]. The shape of the waveform reflected a one-electron process, despite the fact that oxidation of sulfite to sulfate is a two-electron oxidation, and it was concluded that the behavior reflected the catalytically limiting intramolecular transfer of reducing equivalents from the molybdenum center to the heme within the enzyme. Given that the amplitude of the catalytic wave indicated only ~5% of the immobilized enzyme was engaged in turnover, it was concluded that the enzyme was immobilized with its heme domain proximal to the electrode surface with no direct electrochemical contact between the molybdenum center and the electrode, with only a small portion of the enzyme population was considered to be in a configuration where the two redox-active centers of the enzyme were close enough for intramolecular electron transfer to occur. More recently, sulfite oxidase and cytochrome *c* have been coimmobilized in molecular layers onto a specially treated electrode possessing a monolayer of cytochrome *c* [195]. While a layer of enzyme appears to promote deposition of a second layer of cytochrome *c*, this and subsequent layers of the cytochrome appear to be insulated from the electrode-proximal monolayer. Addition of sulfite results in a catalytic wave that can be observed even at very rapid scan rates, indicating that the enzyme, once reduced by sulfite, efficiently passes electrons on to cytochrome *c* then on to the electrode. The catalytic current is dependent on sulfite concentration below 2 mM, with an effective K_m of approximately 310 μM. Unfortunately, no estimation was made of the proportion of immobilized enzyme molecules that were catalytically active.

4.4. The oxidative half-reaction

The reductive half-reaction of the catalytic cycle for the vertebrate and plant sulfite oxidases is thought to proceed in fundamentally the same way, as described above. The oxidative half-reaction, on the other hand, is necessarily different since electrons depart the vertebrate enzyme via its heme, which is absent in the plant enzyme. With chicken sulfite oxidase, the reaction of reduced enzyme with cytochrome *c* exhibits hyperbolic dependence on [cyt *c*] throughout the pH range 6.0–10, with the limiting rate of reaction varying from 130 s^{-1} at pH 6.0 to approximately 600 s^{-1} above pH 8, with an apparent pK_a of 6.8 [181]. k_{ox}/K_d, on the other hand, exhibits a bell-shaped pH dependence with pK_as of 8.0 and 8.2, and a maximum value of 8.0×10^7 M^{-1} s^{-1} at 8.0. Given the likely complexity of the interaction between cytochrome *c* and the heme domain of sulfite oxidase, no attempt was made to assign these pK_as to specific amino acid residues (which could be on either protein). It is known, however, that a group of lysine residues (in particular Lys 13, 27, 72 and 86) that ring the exposed surface heme edge of cytochrome *c* is important in the interaction of cytochrome *c* with sulfite oxidase [196]. An examination of the structure of the chicken enzyme indicates that Tyr 62, Glu 67 and Glu 72 are all on the face of the heme domain on which one edge (that possessing the two heme propionate side chains) is exposed. These residues, as well as the heme propionates themselves, are likely important in the interaction with the positively charged face of cytochrome *c* [187].

For plant sulfite oxidase, the enzyme was initially reported on the basis of steady-state assays to react with O_2 directly, and that H_2O_2 was the product of the reaction [197]. More recently, it has been demonstrated that H_2O_2 is formed only indirectly, by the spontaneous dismutation of $O_2^{\bullet -}$ which is the immediate product of the reaction. The observed rate constant for the reaction exhibits a linear dependence on [O_2], with an apparent second-order rate constant of 5.3×10^4 M^{-1} s^{-1} at pH 8.0 [198]. With a rate of reduction by sulfite that exceeds that accessible by stopped-flow [163], the oxidative half-reaction is clearly rate-limiting for overall turnover with the plant enzyme. Given the localization of plant sulfite oxidase in the peroxisome, it is possible that superoxide generated by it is involved in antimicrobial generation of reactive oxygen species, although an appropriate source of sulfite to provide the reducing equivalents necessary for generation of a superoxide burst upon infection has not been identified. The structural basis of the oxygen-reactivity of the plant sulfite oxidase, which is quite unusual for a molybdenum center, has not been elucidated, although among the very few differences in the environments of the molybdenum centers of sulfite oxidase family members, Tyr 49 in the plant sulfite oxidase is a Phe in chicken and human sulfite oxidases (and also in nitrate reductase, see below). In addition to a possible physiological role for plant sulfite oxidase in microbial defense mechanisms, it has been shown that over expression of the enzyme imparts resistance to air-borne SO_2 [199,200], and the primary role for the enzyme may well be detoxification rather than biological defense.

4.5. Pulsed EPR studies of sulfite oxidase

The Mo(V) state of chicken sulfite oxidase has been extensively studied, with three basic forms of EPR signal being designated on the basis of the conditions under which they are generated.

These are [171]: "low-pH", "high-pH" and "phosphate-inhibited". The "low-pH" signal is distinguishable on the basis of strong hyperfine coupling to a solvent-exchangeable proton that is absent at high pH. The *A. thaliana* enzyme differs from the chicken and human enzymes in not forming a "phosphate-inhibited" EPR signal, and in not showing evident proton coupling in the "low-pH" signal [165]; the basis for this latter observation is discussed further below. Over the past 12 years, Enemark and coworkers have applied variable-frequency pulsed EPR and ENDOR methods to probe the immediate environment of the molybdenum of sulfite oxidase for protons and other magnetically active nuclei. It has been demonstrated, for example, that a solvent-exchangeable and strongly but very anisotropically coupled proton is present in the "high-pH" species of chicken sulfite oxidase, probably a Mo–OH/D group as assigned in the "low-pH" signal [201,202]. The difference in the extent of coupling is ascribed to differences in orientation of the bent Mo–O–H moiety, with the proton situated in a node of the singly-occupied d_{xy} orbital at low pH, and rotated out of it at high pH. Interestingly, and paradoxically, evidence was found for a second exchangeable proton in the high-pH form only, ascribed to HO^- occupying in the substrate binding site that hydrogen-bonded to the Mo–OH group [201,202]. Both of the protons detected in the high-pH signal exhibited a range of coupling constants, suggesting a (limited) distribution of configurations in the signal-giving species. By contrast, the strongly coupled proton in the low-pH species was more conformationally constrained, possibly due to a hydrogen-bonding interaction between the Mo–OH and the cysteine sulfur coordinating to the molybdenum [202]. A subsequent pulsed ENDOR and EPR study of the low-pH signal has identified the non-exchangeable C_α proton of the liganded Cys 185/207 in both chicken and human sulfite oxidases, at a distance of 2.8 Å [203]. This distance increased to 3.3 Å in the high-pH signal, attributed to a modest change in the torsional angle of the liganded cysteine itself relative to the molybdenum ligand field.

It has been known for many years that a strongly coupled oxygen from ^{17}O-labeled solvent exchanged into the molybdenum center of sulfite oxidase in both the low-pH and high-pH forms, and while initially ascribed to a terminal Mo=O group [204], subsequent resonance Raman work [205] has been interpreted as indicating that this site is the equatorial Mo–OH rather than apical Mo=O in the signal-giving Mo(V) species. More recently, pulsed EPR work has confirmed this more strongly coupled oxygen and provided evidence for a second, more weakly coupled but still solvent exchangeable, oxygen assigned to the apical Mo=O ligand in the molybdenum center [206]. This interpretation runs counter to the original resonance Raman study with the chicken enzyme, however, which concluded on the basis of the magnitude of the isotope shift on incorporation of ^{18}O into the molybdenum center that only a single site had become labeled [205]. More recently, the resonance Raman of the *A. thaliana* sulfite oxidase has been examined, taking advantage of the absence of a heme site in the protein [165]. In the 800–1000 cm^{-1} region where Mo=O stretches are to be expected, three strong lines are observed at 896, 877 and 864 cm^{-1} using 488-nm excitation. The 896 and 864 cm^{-1} modes were, by analogy to comparable modes seen at 903 and 881 cm^{-1} with the chicken enzyme, to symmetric and antisymmetric stretching modes of the MoO_2 unit of the molybdenum center, and the 877 cm^{-1} band to a vibrational mode having mixed enedithiolate and pyran ring character. The improved signal-to-noise obtained with the plant protein made it possible to establish an approximately two-fold greater intensity of the symmetric vibrational mode relative to the antisymmetric mode, a fact that necessarily reflects the redox-active orbital arising from an antibonding interaction between the Mo d_{xy} and an O p orbital of the equatorial Mo=O, specifically [165]. After redox-cycling in $H_2{}^{18}O$ to incorporate label into the active site, the 896 and 864 cm^{-1} modes shifted to 854 and 825 cm^{-1}; a band at 910 cm^{-1} was also clearly resolved, evident in the ^{16}O sample as a shoulder on the 896 cm^{-1} mode, as was a second band at 883 cm^{-1}. Unfortunately, it was not possible to distinguish whether one or both of the Mo=O oxygens were exchanged in the experimental protocol used. If only the equatorial oxygen is labeled, then the 825 cm^{-1} mode would represent the isotope-sensitive υ_{eq} mode, with a shift of 39 cm^{-1} from the υ_{as} at 864 cm^{-1} that is near the 44 cm^{-1} expected for a simple harmonic oscillator. This analysis explicitly takes into account the fact that substitution of only one of the oxygens in the MoO_2 unit breaks the symmetry of the center, making it necessary to consider equatorial and apical vibrational modes explicitly, rather than symmetric and antisymmetric modes. Alternatively, in the case where both oxygens become labeled, υ_s and υ_{as} modes are again applicable, and it is possible to assign these to the observed bands at 854 and 825 cm^{-1}, respectively (each shifted by approximately a factor of approximately 0.95 – determined from small-molecule work – from the υ_s = 896 and υ_{as} = 864 modes seen in unlabeled enzyme). It is thus possible to interpret the Raman data using either singly- or doubly-labeled models and it is at present not possible to distinguish unambiguously whether the apical oxo group is in fact solvent-exchangeable.

Less controversially, a pulsed EPR study using ^{33}S-labeled sulfite to generate the low-pH species of the *A. thaliana* sulfite oxidase has provided clear evidence for sulfate coordinated to molybdenum, with an extremely strong ^{33}S amplitude in the two-pulse ESEEM trace. The signal-giving species generated under the experimental conditions used (reduction by sulfite followed with partial reoxidation by ferricyanide) also lacks the strongly coupled proton typically seen in the "low-pH" EPR signal [206] (which had also been seen previously under at least certain conditions with the chicken enzyme [4,207]), and has been interpreted as a $LMo^{V}O(O–SO_3{}^-)$(S-Cys) center with product sulfate coordinated to the molybdenum. The *g*-values for this species in which product is "blocked" from dissociation are $g_{1,2,3}$ = 2.005, 1.974, 1.963, virtually indistinguishable from the parameters for the ordinary "low-pH" spectrum (generated by reduction of enzyme with $Ti^{III\bullet}$ citrate), $g_{1,2,3}$ = 2.006, 1.975, 1.968. This is precisely the intermediate expected for a reaction mechanism proceeding via lone-pair attack on the equatorial Mo=O of the oxidized enzyme. Interestingly, a Y343F mutant in human sulfite oxidase also predisposes this "blocked" low-pH EPR signal (and also results in an increase in the pK_a associated with the low-pH/high-pH interconversion) [208].

Chloride is a well-established inhibitor of the vertebrate sulfite oxidases, and is known to influence the pH-dependent interconversion of the low-pH and high-pH forms of the Mo(V) state in a way that suggests it binds to the former but not the latter [209]. On the basis of a comparison of the low-pH continuous-wave EPR spectra obtained in the presence of $Na^{35}Cl$ and $Na^{37}Cl$ (both having I = 3/2, but ^{35}Cl has a ~20% larger nuclear magneton), distinct hyperfine coupling was detected that was interpreted as evidence for direct coordination of chloride to molybdenum at the vacant ligand position *trans* to the apical Mo=O group [210]. A second study utilizing pulsed EPR in conjunction with density functional calculations, however, has concluded that the observed magnitude of both the hyperfine and nuclear quadrupole interaction parameters for ^{35}Cl strongly support a structure for the signal-giving species in which chloride is not directly coordinated to the molybdenum but rather bound in the substrate binding site and hydrogen-bonding to the Mo–OH [211]. The latter interpretation is consistent with the subsequently determined X-ray crystal structure of the recombinant chicken enzyme, showing chloride in the substrate binding site [59d]. Very recently, the effect of chloride on the "low-pH" EPR signal of both human and *A. thaliana* sulfite oxidases, as well as a closely related sulfite dehydrogenase from the bacterium *S. novella*, has demonstrated that depletion of chloride results in accumulation of the "blocked" form of the low-pH signal that lacks strong

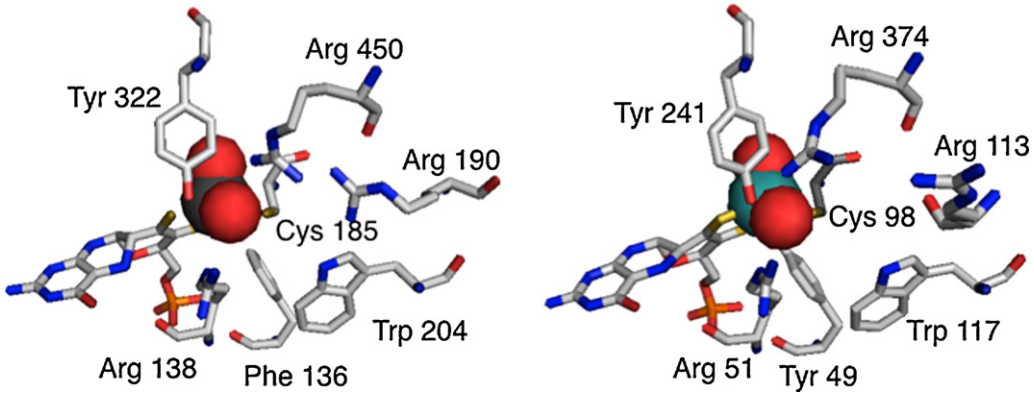

Fig. 14. The active sites of chicken (left) and *A. thaliana* (right) sulfite oxidases. The perspective is looking into the active site from the solvent access channel, with the apical Mo=O of the molybdenum center oriented vertically. The distinctly different orientations of Arg 460/374 in the two structures are to be noted.

proton hyperfine coupling and has sulfate trapped on the molybdenum [212]. In the human enzyme, the "blocked" form exhibits rather different *g*-values ($g_{1,2,3}$ = 1.999, 1.972, and 1.963) than the ordinary "low-pH" form ($g_{1,2,3}$ = 2.004, 1.973, and 1.966). It has been concluded that chloride promotes hydrolysis of the Mo–O–SO_3^- bond and appearance of the characteristic proton doublet of the unblocked low-pH signal (although only incompletely in the case of the plant enzyme). The R160Q mutant of the human protein remains locked in the "blocked" configuration even in the presence of 100 mM chloride, indicating that in addition to its dramatically attenuated intramolecular electron transfer rate (above) the mutant is also compromised in completing the chemistry of the reductive half-reaction [213]. Given the structural work with the wild-type and R138Q chicken enzyme [167], it is evident that the "blocked" and "unblocked" forms of the enzyme differ predominantly in the position of Arg 450, with this residue facing into or away from the substrate binding sites, respectively. The observed binding of chloride in the substrate binding pocket provides an obvious basis by which the anion might influence the equilibrium position of Arg 450. Still, it must be borne in mind that the *A. thaliana* enzyme, crystallized with the corresponding Arg 374 in an "open" or "unblocked" position is very predisposed to the "blocked" form on the basis of the ease with which a "low-pH" EPR signal lacking proton hyperfine is observed.

5. Nitrate reductase

5.1. Introduction to structure

Assimilatory nitrate reductase catalyzes the first (and rate-limiting) step in the uptake of nitrate by fungi, algae and higher plants [214–216]. The enzyme is a member of the sulfite oxidase family of molybdenum enzymes and has the same square-pyramidal $LMo^{VI}O_2$(S-Cys) molybdenum center in the oxidized enzyme. Pyridine nucleotides are the source of reducing equivalents for catalysis by all nitrate reductases: the enzyme from higher plants utilizes NADH, while that from fungal sources is specific for NADPH. The algal enzymes are typically specific for NADH, although some non-specific enzymes able to utilize either NADH or NADPH have been described [214].

Nitrate reductase from *A. thaliana* and other higher plants is a homodimer of 2 × 110 kDa. Each subunit consists of a large N-terminal portion (~59 kDa) that possesses the molybdenum center, a small central domain possessing a *b*-type cytochrome (14 kDa), and a C-terminal domain containing FAD and the NADH binding site (24 kDa) [217]. In the course of turnover, NADH introduces reducing equivalents into the enzyme at its FAD site and these are subsequently transferred via the heme to the molybdenum center, where nitrate is reduced [214–216]. The molybdenum- and heme-containing domains have significant sequence and structural homology to the cognate portions of the eukaryotic sulfite oxidases and cytochrome b_5, respectively, and the flavin-binding portion to members of the large ferredoxin:$NADP^+$ reductase family of flavoproteins [6].

The structure of holo nitrate reductase remains unknown, but crystal structures for the molybdenum domain from the *Pichia angusta* enzyme [218], for bovine cytochrome b_5 [219,220] and the flavin domain from *Zea mays* nitrate reductase [221] have all been reported (Fig. 15). The molybdenum domain from *P. angusta* bears a striking resemblance to the corresponding portion of that of both the chicken [161] and *A. thaliana* [162] sulfite oxidases, with molybdenum-binding and dimerization subdomains. As with the sulfite oxidases, the equatorial Mo=O of the oxidized molybdenum coordination sphere faces into the solvent access channel to the active site. The substrate binding site (Fig. 16) consists of two arginine residues, Arg 89 and 144, as well as Trp 158, all three of which are structurally conserved with the sulfite oxidases. The substrate binding site also includes Met 427 (a Val in the sulfite oxidases), Asn 272 (a Tyr in the sulfite oxidases) and Thr 425 (an Arg in the sulfite oxidases) that impart substrate specificity. The orientation of the molybdenum, heme and flavin domains with respect to one another in the holoenzyme is at present unknown.

5.2. Kinetic behavior

The basic chemistry of nitrate reduction is believed to be straightforward, and functionally the reverse of the oxygen atom transfer seen with sulfite oxidase, with nitrate serving as oxygen atom donor and the reduced molybdenum center functioning as the oxygen atom acceptor:

$$O{=}NO_2^- + LMo^{IV}O(OH)(S\text{-}Cys) \rightarrow : NO_2^- + LMo^{VI}O_2(S\text{-}Cys) + HO^-$$

Reduction of the $LMo^{VI}O_2$(S-Cys) core of the active site yields LMo^{IV}O(OH)(S-Cys), consistent with X-ray absorption studies of the enzyme [222,223]. With each catalytic cycle, the equatorial Mo=O (after reduction, protonation and displacement by nitrate) is thought to be lost to solvent, and is subsequently regenerated with oxygen derived from substrate in the oxygen atom transfer event. The basis for the nitrate-utilizing enzyme being a reductase and the sulfite-utilizing enzyme an oxidase has been accounted for on thermodynamic grounds and the relative stabilities of N=O, S=O and Mo=O bonds [224]. As in the case of sulfite oxidase, unfortunately, there is to date no direct experimental evidence for an oxygen atom transfer mechanism as envisaged by this mechanism.

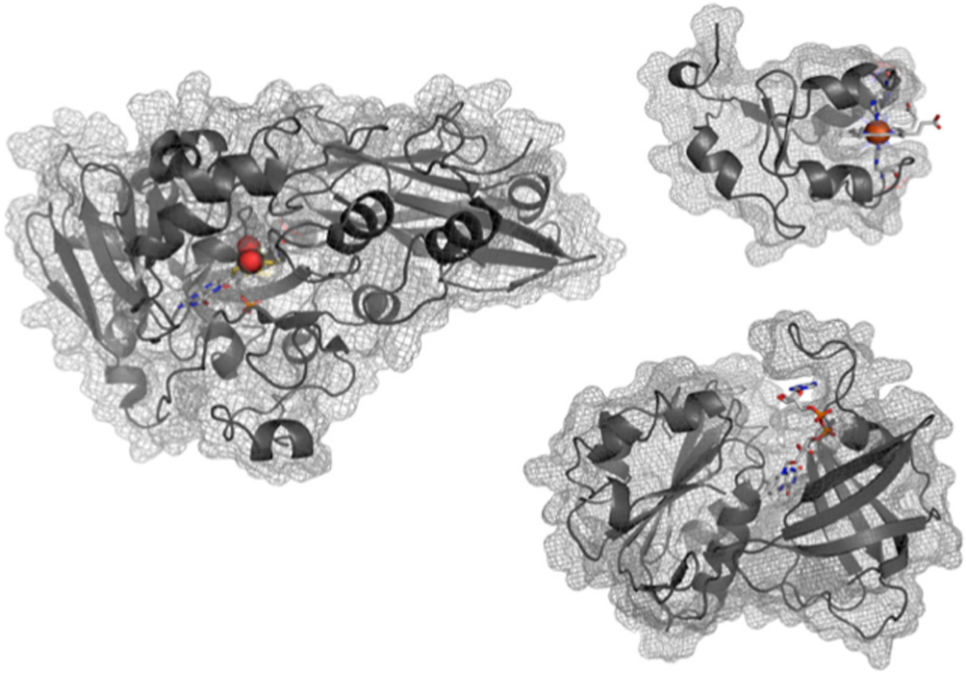

Fig. 15. *Structures of the three domains of nitrate reductase*. Shown are ribbon representations of the polypeptide backbone with the protein surface rendered in mesh. Cofactors are rendered in CPK coloring and metal centers rendered as spheres. *Left*, the molybdenum domain from *Pichia angusta*, looking down the solvent access channel to the Mo center (Cys 139, coordinating the molybdenum, lies to the right of the metal). As shown, the dimerization subdomain for the α_2 holoenzyme lies to the right of the molybdenum-binding subdomain. *Right* (*top*), the heme domain of rat cytochrome b_5. *Right* (*bottom*), the flavin domain from corn, with the NADH binding cleft at top, above the FAD cofactor.

The steady-state kinetics of several plant nitrate reductases have been summarized previously [94–96]. The specific steady-state kinetic parameters for the *A. thaliana* enzyme are $k_{cat} = 210\,s^{-1}$; $K_m^{nitrate} = 90\,\mu M$; and $K_m^{NaDH} = 0.8\,\mu M$ at pH 7.0, 30 °C [225]. More detailed rapid reaction kinetic analysis of the enzyme's behavior has been limited by the low availability of the enzyme, although in the past decade progress has been made in the development of suitable expression systems of individual domains of nitrate reductase and, most recently, the holoenzyme. The reaction of the flavin fragment of corn nitrate reductase, and also a mutant in which the highly conserved Cys 242 is replaced with a serine residue (C242S), with NADH has been examined [226]. For both wild-type and mutant protein, the observed rate constant for the reaction exhibits a hyperbolic dependence on [NADH] – the limiting rate constant for reduction at high [NADH] for the C242S mutant is some seven-fold slower than that for the wild-type protein ($68\,s^{-1}$ as compared with $478\,s^{-1}$) and K_d^{NaDH} is larger by a factor of 2 ($6\,\mu M$ vs. $3\,\mu M$). It is evident that Cys 242 plays a modest role in facilitating electron transfer from NADH to the flavin and only a minimal role in binding of NADH to the enzyme, its mutation to Ser reducing k_{red}/K_d^{NaDH} by a factor of just over 10 [226]. Interestingly, the product of the reaction is not free reduced protein but

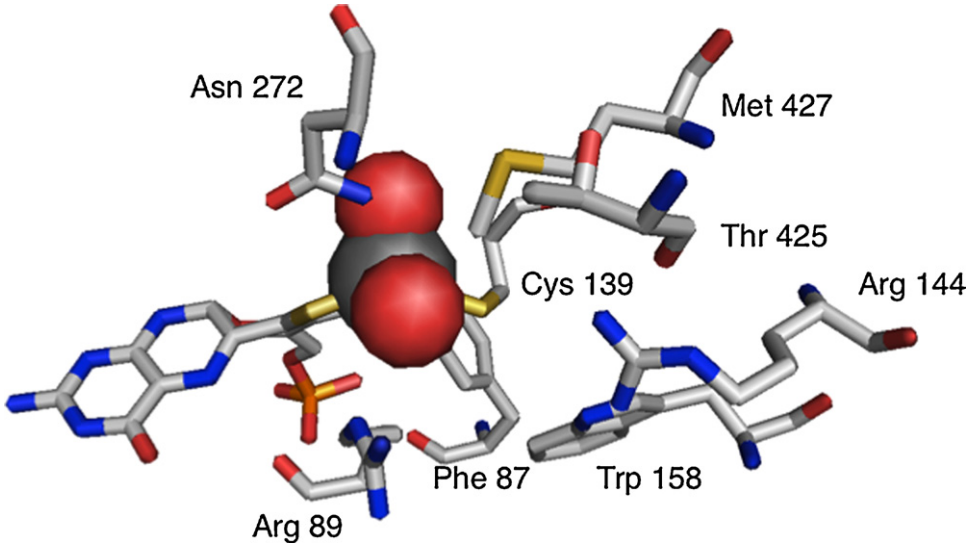

Fig. 16. The active site of *Pichia angusta* nitrate reductase. The perspective is the same as shown in Fig. 14 for the structures of the chicken and *A. thaliana* sulfite oxidases, for purposes of comparison.

rather an $FADH_2$•NAD^+ charge-transfer complex that has a characteristic long-wavelength absorption with a maximum at 800 nm ($\varepsilon = 2.7\ mM^{-1}\ cm^{-1}$) [226].

The reaction of a combined flavin-heme fragment of nitrate reductase from spinach with NADH has also been examined [227]. The reaction is multiphasic, with a fast phase whose spectral change indicates formation of the same $FADH_2$•NAD^+ complex as seen with the flavin fragment alone. k_{obs} again exhibits a hyperbolic dependence on [NADH] with a k_{red} of $560\ s^{-1}$ and a K_d of 3 μM, in good agreement with the results using the (corn) flavin fragment alone ($478\ s^{-1}$ and 3 μM, respectively). Surprisingly, the subsequent internal electron transfer from $FADH_2$ to heme was very slow, $12\ s^{-1}$, and appeared to be rate-limited by dissociation of NAD^+ from the E_{red}•NAD^+ charge-transfer complex. The slowest phase of the reaction was attributed to an intermolecular disproportionation of the two-electron reduced protein formed after reaction with a first equivalent of NADH reacts to yield one equivalent each of the one- and three-electron reduced form (the former then reacting with a second equivalent of NADH to give further reduction).

The rapid reaction kinetics of holo nitrate reductase from *A. thaliana* has also been examined [228] (a preliminary report of this work had also appeared [229]). The kinetics of enzyme reduction by NADH largely confirmed the above results with the flavin-heme fragment, with a fast phase of $\sim 700\ s^{-1}$ observed at 70 μM NADH that corresponded to reduction of $FADH_2$, and a subsequent slower phase at $28\ s^{-1}$ corresponding to electron transfer on to the heme. No evidence was found for formation of an $FADH_2$•NAD^+ charge-transfer complex, however, and its role in catalysis has not been confirmed. A significant amount of heme reduction was observed in the fast phase of the reaction, however, and again no evidence of a charge-transfer complex at the flavin site was observed. Together the two results are at least internally consistent, in that electron transfer from the flavin on to the heme would be expected to be fast absent a charge-transfer complex to retard oxidation of the flavin, but it is surprising that the complex would be so readily observed in the case of the corn [226] or spinach [227] proteins and not form at all in the *A. thaliana* protein. Somewhat surprisingly, the kinetics of the reoxidation of pre-reduced nitrate reductase with nitrate were not examined in this study, perhaps owing to the inevitable complications due to the fact that only ~20% of the protein possessed a molybdenum center. A series of enzyme-monitored turnover experiments were performed, however, in which enzyme at a concentration of, for example, 2 μM enzyme pre-reduced with 40 μM NADH was reacted with 90 μM nitrate. The kinetics for the approach to steady-state, as followed by the absorbance changes at 460 nm (following changes in the oxidation state of the FAD) and 557 nm (following changes in the oxidation state of the heme), were biphasic with apparent rate constants of $260–270\ s^{-1}$ and $6–8\ s^{-1}$, respectively. The steady-state persisted for over 1.0 s, with the FAD held at 84% reduced and the heme 42% (presumably reflecting the distribution of reducing equivalents in the partially reduced enzyme in the steady-state). At the end of the steady-state, with the NADH presumably depleted and 50 μM nitrate remaining in solution, the enzyme slowly reoxidized with an apparent rate constant of $0.5\ s^{-1}$. This last value is unfortunately too slow to support turnover, and the possibility exists that most of the observed kinetics the large proportion of enzyme lacking a molybdenum center (which, despite being readily reducible by NADH, could not be reoxidized by nitrate) was slowly passing reducing equivalents to the small population of enzyme that was functional and could react with nitrate. The implication is that the magnitude of the absorbance changes seen in the initial approach to steady-state meant that the functional enzyme had become essentially completely reoxidized, which would require that the reoxidation of enzyme with nitrate was considerably faster that its rate of reduction by NADH.

5.3. Post-translational regulation

The activity of assimilatory nitrate reductases is under tight control, and includes regulation at the transcriptional, translational and post-translational levels [214–216]. The last plays an important role in lowering nitrate reductase activity at night, when photosynthetically generated reducing equivalents are not available to reduce nitrite on to ammonia, as nocturnal nitrite levels in the plant tissues would otherwise increase to dangerous levels [230]. This post-translational regulation of nitrate reductase involves phosphorylation at a serine residue in the linker region between the molybdenum and heme domains [231]; the modified residue has been identified as Ser 543 in the spinach protein [232] (equivalent to Ser 534 of the *A. thaliana* enzyme). Phosphorylation is carried out by any one of several specific protein kinases (including AMP-activated protein kinase [98] and calcium-dependent protein kinase, CDPK [233]). Phosphorylation does not directly inhibit activity, but rather creates a recognition site that recruits a specific regulatory element, a member of the 14-3-3 family of proteins, whose binding (in the presence of Mg^{2+}, which is required for inhibition) effectively shuts down activity [234]. Of the twelve isoforms of 14-3-3 protein that have been identified in *A. thaliana*, the isoform has proven to be particularly effective in binding to and inhibiting the phosphorylated form of nitrate reductase [235].

Most recently, the steady-state kinetic properties of *A. thaliana* nitrate reductase in as-isolated, phosphorylated and phosphorylated-(14-3-3)ω complexed forms have been investigated [236]. Of the several calcium-dependent protein kinases encoded by the *A. thaliana* genome, CPK-17 efficiently phosphorylated nitrate reductase at Ser 534 *in vitro* (other secondary sites were also identified, although these were only ineffectively phosphorylated by CPK-17). Similarly, of the several 14-3-3 proteins in *A. thaliana*, the ω and λ isoforms bound phosphorylated nitrate reductase with highest affinity (K_i = 60 and 80 nM, respectively). In NADH-nitrate assays, the as-isolated enzyme exhibited a k_{cat} of $20\ s^{-1}$, $K_m^{nitrate}$ of 197 μM and K_m^{NaDH} of 18 μM, phosphorylated enzyme exhibited a somewhat higher k_{cat} and $K_m^{nitrate}$ of $33\ s^{-1}$ and ~200 μM, respectively, while the phosphorylated enzyme complexed with 14-3-3ω gave a substantially reduced k_{cat} of $1.8\ s^{-1}$ and $K_m^{nitrate}$ of 141 μM. An S534A mutant of the nitrate reductase was not inhibited by 14-3-3ω, underscoring the importance of the phosphorylated site in formation of the inhibitory complex. Significantly, phosphorylation and 14-3-3ω binding had no effect on turnover with NADH and cytochrome *c* as substrate. Cytochrome *c* accepts reducing equivalents from nitrate reductase at the heme site of the latter, and the kinetic results indicate that neither the reductive half-reaction nor electron transfer from the flavin to the heme are affected by 14-3-3ω binding. Similarly, 14-3-3ω binding did not influence K_i for product nitrite, and it was concluded that substrate binding similarly would be unaffected (as suggested by the only modest changes in $K_m^{nitrate}$ seen in the steady-state assays). It has been concluded that the most likely basis for 14-3-3ω inhibition of the phosphorylated nitrate reductase is either the reduction of nitrate at the reduced molybdenum center or (more likely) reduction in the rate of electron transfer from the heme to the molybdenum in the enzyme.

6. Mitochondrial amidoxime reducing component

6.1. Substrates and distribution

The third and final component of an NADH-utilizing system capable of reducing a wide range of hydroxylated amine substrates has recently been found to be a molybdenum-containing enzyme [7,8]. As the name suggests, mitochondrial amidoxime

reducing component (mARC) proteins are localized in or are associated with mitochondria, where they catalyze the reduction of diverse *N*-hydroxylated substrates such as amidoximes, *N*-hydroxy-sulfonamides and *N*-hydroxy-guanidines, many of which are utilized as prodrugs for therapeutic purposes (having greater membrane permeability than the readily protonated amine groups themselves) [7,8,237]. While the true physiological substrate(s) are as yet unknown, a few of the tested *N*-hydroxylated compounds are likely to be of physiological relevance. The *N*-hydroxylated base analogue *N*-hydroxy-cytosine is reduced to cytosine with high efficiency by human mARC proteins, providing a mechanism for detoxification of these base analogs which otherwise would be mis-incorporated into DNA and cause accumulation of mutations [237]. Such a detoxification function has been demonstrated for the bacterial MOSC domain proteins YcbX and YiiM, which afford resistance to 6-*N*-hydroxylaminopurine [238]. Mutagenesis of the *ycbX* and *yiiM* genes rendered the bacteria sensitive to 6-*N*-hydroxylaminopurine, with rapid accumulation of mutations and cell death.

The ability of human mARC proteins to reduce the nitric oxide precursor N^4-hydroxy-L-arginine [239] suggests another physiological role of mARC proteins. Nitric oxide is a physiological mediator with diverse functions in, *e.g.*, maintenance of vascular homeostasis, neuronal signaling and inhibition of tumor cell growth. However, overproduction of nitric oxide can lead to cellular damage and a number of serious conditions. Tight control of nitric oxide by nitric oxide synthases, which catalyze the oxidation of L-arginine to L-citrulline and nitric oxide via the intermediate N^4-hydroxy-L-arginine, is therefore crucial for the cell. In this respect, mARC proteins may have an important function in the regulation of intracellular nitric oxide levels by controlled elimination of the nitric oxide precursor N^4-hydroxy-L-arginine.

All annotated genomes of eukaryotes that require molybdenum appear to possess two copies of mARC genes, with both copies showing strong similarities on nucleotide and amino acid levels. Nevertheless, according to certain conserved motives, mARC-1 and mARC-2 proteins can clearly be discriminated, suggesting that each protein has a specific function. Indeed, different substrate preferences have been shown for the two human isoforms [7,239,240] and in different mouse tissues such as kidney and liver the mARC isoform 2 was highly abundant whereas the isoform 1 could hardly be detected [237]. Consistent with this, during several attempts to isolate mARC proteins from the outer membrane of pig liver mitochondria [7] and membrane fractions of *A. thaliana* mitochondria yield isoform 2 exclusively [Wahl, Mendel, Bittner, unpublished data]. Still, not even the sub-cellular localization of mARC proteins is fully defined, since in addition to the outer mitochondrial membrane, mammalian mARC proteins have also been found in the inner mitochondrial membrane [241] as well as in peroxisomal membranes [242].

6.2. The molybdenum centers of eukaryotic mARC enzymes

Based on sequence similarity, mARC proteins are related to the molybdenum cofactor sulfurases C-terminal (MOSC) domains of ABA3 and related sulfurase systems, their main structural features being a β-barrel-like structure N-terminal to the MOSC domain itself, and a strictly conserved cysteine residue (Cys 273 and Cys 272 in human mARC proteins) at the extreme C-terminal end [243]. The β-barrel-like structure is predicted to have specific roles in the interaction with the substrates of MOSC domain proteins, while the conserved cysteine residue accepts sulfur from the sulfur-generating systems such as cysteine desulfurases prior to transfer on other proteins for yet unknown scopes. Since the molybdenum cofactor sulfurases involved in formation of a Mo=S center for xanthine oxidase family enzymes consist a sulfur-generating cysteine desulfurase domain as well as a MOSC domain, MOSC domain proteins including mARC and bacterial YiiM-like proteins are generally thought to be involved in metal–sulfur cluster biogenesis [243], although this has yet to be determined experimentally.

mARC proteins represent the simplest eukaryotic molybdenum enzymes in that they consist of only a single distinct MOSC domain and bind only one prosthetic group, the molybdenum cofactor. Moreover, with a average molecular weight of 35 kDa mARCs are even smaller than that of plant sulfite oxidase and, in contrast to all other known eukaryotic molybdenum enzymes, which are dimers, mARC proteins are monomeric [237]. Our current knowledge on mARC proteins suggests that they are not active as stand-alone proteins, but rather act in concert with other redox-active proteins, specifically cytochrome b_5 and the FAD-binding NADH:cytochrome b_5 reductase [7,8,237,240]. The complement of redox-active centers in this three-protein complex resembles that seen in nitrate reductase (see Section 5), with the same direction of electron transfer through the system: NADH to FAD to cytochrome b_5 to molybdenum. It remains to be seen whether deeper structural homologies exist.

Another important aspect concerns the structure of the molybdenum center in eukaryotic mARC proteins and probably all proteins of the MOSC domain superfamily. In contrast to the $LMo^{VI}OS(OH)$ and $LMo^{VI}O_2$(S-Cys) molybdenum centers of xanthine oxidoreductase and sulfite oxidase family enzymes, respectively (see Sections 2 and 4), the molybdenum centers of human mARC proteins neither coordinate an equatorial sulfido ligand nor a cysteine sulfur [237]. This has been demonstrated on the one hand by cyanide treatment which neither released sulfur in the form of thiocyanate nor significantly affected the activities of the human mARC proteins. Consistent with this, co-incubation of apo-mARC proteins with a cofactor-loaded molybdenum cofactor carrier protein that binds the cofactor in a $LMoO_2(OH)$ form reconstituted the activity of the mARC proteins. Both experiments confirmed that human mARC proteins do not require a sulfurated cofactor as present in xanthine oxidase family enzymes. On the other hand, partially reduced human mARC proteins developed EPR signals characteristic of the Mo(V) (d^1) state. The signals of the two investigated mARC isoforms were very similar, with rhombic symmetry, $g_{av} \sim 1.975$ and approximately isotropic superhyperfine coupling to a single exchangeable proton. Both spectra closely resembled the so-called "low pH" EPR signal seen with sulfite oxidase and, in particular, nitrate reductase. However, mutation of each of the 10 cysteine residues in human mARC proteins did not perturb the EPR spectra to any significant degree nor was the activity of the mutated enzymes affected. Thus, the (human) mARC proteins cannot be regarded as members of the sulfite oxidase family as they do not provide a cysteine sulfur to the molybdenum center. There are two likely possibilities for the Mo coordination sphere of mARC proteins. The first is a trioxo species $LMo^{VI}O_3$ that protonates upon reduction to $LMoO_2(OH)$. The second is an $LMoO_2X$ species, with X being either an as yet unknown inorganic or, alternatively a protein-derived ligand other than cysteine. In either case, the coordination of the molybdenum in the cofactor of mARC proteins differs fundamentally from that seen in enzymes of the sulfite oxidase and xanthine oxidase families and thus likely represent a new family of molybdenum enzymes distinct from the well-known sulfite oxidase and xanthine oxidase families.

7. Concluding remarks

It is evident from the above that over the past 10–15 years our progress in understanding molybdenum-containing enzymes from eukaryotes has been striking. At the same time, one can expect much progress in the immediate future. The specific cat-

alytic roles of amino acid residues in the active site of xanthine oxidoreductase will be clarified, and increasingly effective therapeutic agents targeting the enzyme will be developed, possibly including some with efficacy in the treatment of conditions such as ALS, Parkinson's Disease and Alzheimer's. There will also be advances in our understanding of the physiological role(s) of aldehyde oxidase and its homologs in both plants and mammals, as well as the possible involvement of these enzymes in the generation of reactive oxygen species under a variety of pathophysiological conditions. The workings of sulfite-oxidizing enzymes (in prokaryotes as well as eukaryotes) will be better elucidated, including for example a better understanding of the structural basis for the reactivity of the molybdenum center of the plant sulfite oxidase toward O_2 and the detailed manner in which the physical structure of the molybdenum center determines its electronic structure (and therefore reactivity). We can also expect that the kinetic behavior of nitrate reductase from higher plants will be increasingly well understood, and the basis for its diurnal regulation established. Site-directed mutagenesis studies of active site amino acid can be expected to establish the basis for substrate specificity in the sulfite oxidases and nitrate reductases, and possibly generate new forms with altered reactivity. Further characterization of the mARC proteins can be expected to clarify the relationship of these and related proteins to the established families of molybdenum-containing enzymes and determine whether these constitute a previously unrecognized family of these enzymes, and also what their physiological roles are in the cell. Finally, genomics and proteomics approaches hold out the promise that new molybdenum-containing enzymes, even new families of enzymes, will be identified.

Note added in proof

After the original submission of this article, two crystal structures of urate bound to XDH have been reported [244]. These authors determined the structures of the urate complexes of the demolybdo-form of the D428A mutant of rat XOR at 1.7 Å and of reduced bovine milk XOR at 2.1 Å resolutions, respectively. The latter structure was obtained with a crystal grown from the active bovine XDH form which had been soaked with a large excess of NADH under strictly anaerobic conditions in order to reduce other cofactors and to block any electron transfer from the Mo center. The molybdenum center was then reduced by soaking in 4 mM titanium citrate solution and urate added to give a concentration of 250 μM. In the electron density map, the urate molecule locates near the molybdenum and rather high electron density connects the two, suggesting a covalent linkage between molybdenum and urate via a bridging oxygen from urate. The bridging electron density is bent, spanning a total of 3.5 Å and connects to the C8 atom of urate. Placing the oxygen atom at the apex of the bent electron density leads to Mo-O and C8-O distances of 2.2 Å and 1.4 Å, respectively. The urate binding mode seen in both these new structures is inverted relative to the xanthine binding mode seen with desulfo enzyme (67), with a presumably protonated Glu 1261 forming a 3.0 Å long hydrogen bond to N9 of urate And Glu 802 equidistant (2.6 Å) from both N7 and O=C6 of urate. In addition, three water molecules are found within hydrogen bonding distance to urate, with one located near N3 and N9 of urate. The orientation of urate is very similar to that seen the demolybdo-form of rat XOR D428A (above). Superimposing the two structures reveals that all amino acid residues interacting with urate, including the two glutamic acids, arginine and two phenylalanines, differ in position by less than 0.4 Å. The atoms of urate itself, however, are not completely overlapping: the C-8 keto oxygen of urate in to demolybdostructure is in the plane of the imidazole subnucleus, implying sp^2 hybridization of C8, whereas it distinctly out-of-plane in the active site of the completely reduced XOR, implying sp^3 hybridization of C8. However, as the position of the C-8 carbon-atom is the same in both cases, these authors argue that the binding mode of urate to the rat demolybdo-XOR D428A resolved at high resolution (1.7 Å) mimics that of the reaction intermediate of the hydroxylation reaction of xanthine in accordance with the binding mode shown in Fig. 8.

Acknowledgements

The authors wish to thank the National Institutes of Health (GM 075036 and ES 012658 to RH), The Ministry of Education, Culture, Sports, Science and Technology of Japan (Grants 16205021 and 20590317 to TN) and various grants from the Deutsche Forschungsgemeinshaft (to FB) for support of research in their laboratories.

References

[1] E.C. De Renzo, P.G. Heytler, Arch. Biochem. Biophys. 49 (1954) 242.
[2] H.R. Mahler, B. Mackler, D.E. Green, R.M. Bock, J. Biol. Chem. 210 (1954) 465.
[3] D.J.D. Nicholas, A. Nason, W.D. McElroy, J. Biol. Chem. 207 (1954) 341.
[4] H.J. Cohen, I. Fridovich, K.V. Rajagopalan, J. Biol. Chem. 248 (1971) 374.
[5] A. Cvetkovic, A.L. Menon, M.P. Thorgersoen, J.W. Scott, F.L. Poole II, F.E. Jenney Jr., W.A. Lancaster, J.L. Praissman, S. Shanmukh, B.J. Vaccaro, S.A. Trauger, E. Kalisiak, J.V. Apon, G. Siuzdak, S.M. Yannone, J.A. Tainer, M.W.W. Adams, Nature 466 (2010) 779.
[6] R. Hille, Chem. Rev. 96 (1996) 2757.
[7] G. Schwarz, R.R. Mendel, Annu. Rev. Plant Biol. 57 (2006) 623.
[8] A. Havemeyer, F. Bittner, R. Mendel, T. Kunze, B. Clement, J. Biol. Chem. 281 (2006) 34796.
[9] S. Gruenewald, B. Wahl, F. Bittner, H. Hungeling, S. Kranzow, J. Kotthaus, U. Schwering, R.R. Mendel, B. Clement, J. Med. Chem. 51 (2008) 8173.
[10] C. Kisker, H. Schindelin, D.C. Rees, Annu. Rev. Biochem. 66 (1997) 233.
[11] G. Schwarz, R.R. Mendel, M.W. Ribbe, Nature 460 (2009) 839.
[12] J.H. Enemark, A.V. Astashkin, A.M. Raitsimring, Dalton Trans. (2006) 3501.
[13] C. Enroth, B.T. Eger, K. Okamoto, T. Nishino, T. Nishino, E.F. Pai, Proc. Natl. Acad. Sci. U.S.A. 97 (2000) 10723.
[14] M.J. Romão, M. Archer, I. Moura, J.J.G. Moura, J. LeGall, R. Engh, M. Schneider, P. Hof, R. Huber, Science 270 (1995) 1170.
[15] R.M. Jones, F.E. Inscore, R. Hille, M.L. Kirk, Inorg. Chem. 38 (1999) 4963.
[16] H. Dobbek, L. Gremer, R. Kiefersauer, R. Huber, R.O. Meyer, Proc. Natl. Acad. Sci. U.S.A. 99 (2002) 15971.
[17] I. Bonin, B.M. Martins, V. Purvanov, S. Fetzner, R. Huber, H. Dobbek, Structure 12 (2004) 1425.
[18] K. Okamoto, K. Matsumoto, R. Hille, B.T. Eger, E.F. Pai, T. Nishino, Proc. Natl. Acad. Sci. U.S.A. 101 (2004) 7931.
[19] C.J. Doonan, A.L. Stockert, R. Hille, G.N. George, J. Am. Chem. Soc. 127 (2005) 4518.
[20] S.P. Cramer, R. Wahl, K.V. Rajagopalan, J. Am. Chem. Soc. 103 (1979) 7721.
[21] T.D. Tullius, D.M. Kurtz Jr., S.D. Conradson, K.O. Hodgson, J. Am. Chem. Soc. 103 (1979) 2776.
[22] W.H. Orme-Johnson, H. Beinert, Biochem. Biophys. Res. Commun. 36 (1969) 337.
[23] R. Hille, W.R. Hagen, W.R. Dunham, J. Biol. Chem. 260 (1985) 10569.
[24] T. Iwasaki, K. Okamoto, T. Nishino, J. Mizushima, H. Hori, T. Nishino, J. Biochem. 127 (2000) 771.
[25] D.J. Lowe, R.C. Bray, Biochem. J. 169 (1978) 471.
[26] R.E. Coffman, G.R. Buettner, J. Phys. Chem. 83 (1979) 2392.
[27] K.N. Murray, G. Watson, S. Chaykin, J. Biol. Chem. 241 (1966) 4798.
[28] R. Hille, H. Sprecher, J. Biol. Chem. 262 (1987) 10914.
[29] M. Xia, R. Dempski, R. Hille, J. Biol. Chem. 274 (1999) 3323.
[30] R.J. Greenwood, G.L. Wilson, J.R. Pilbrow, A.G. Wedd, J. Am. Chem. Soc. 115 (1993) 5385.
[31] R.B. McWhirter, R. Hille, J. Biol. Chem. 266 (1991) 23724.
[32] S.J. Tanner, R.C. Bray, F. Bergmann, Biochem. Soc. Trans. 6 (1978) 1328.
[33] G.A. Lorigan, R.D. Britt, J.H. Kim, R. Hille, Biochim. Biophys. Acta 1185 (1994) 284.
[34] B.D. Howes, R.C. Bray, R.L. Richards, N.A. Turner, B. Bennett, D.J. Lowe, Biochemistry 35 (1996) 1432.
[35] P. Manikandan, E.-Y. Choi, R. Hille, B.M. Hoffman, J. Am. Chem. Soc. 123 (2001) 2658.
[36] J.M. Pauff, J. Zhang, C.E. Bell, R. Hille, J. Biol. Chem. 283 (2008) 4818.
[37] S. Gutteridge, S.J. Tanner, R.C. Bray, Biochem. J. 175 (1978) 869.
[38] J.H. Kim, M.G. Ryan, H. Knaut, R. Hille, J. Biol. Chem. 271 (1996) 6771.
[39] R. Huber, P. Hof, R.O. Duarte, J.J.G. Moura, I. Moura, J. LeGall, R. Hille, M. Archer, M. Romão, Proc. Natl. Acad. Sci. U.S.A. 93 (1996) 8846.
[40] A. Albert, D.J. Brown, J. Chem. Soc. (1954) 2060.
[41] E.B. Skibo, J.H. Gilchrist, C.-H. Lee, Biochemistry 26 (1987) 3032.
[42] S.C. D'Ardenne, D.E. Edmondson, Biochemistry 29 (1990) 9046.
[43] C.C. Page, C.C. Moser, X. Chen, P.L. Dutton, Nature 402 (1999) 47.

[44] A.L. Stockert, S.S. Shinde, R.F. Anderson, R. Hille, J. Am. Chem. Soc. 124 (2002) 14554.
[45] G. Palmer, R.C. Bray, H. Beinert, J. Biol. Chem. 239 (1964) 2657.
[46] R.C. Bray, G. Palmer, H. Beinert, J. Biol. Chem. 239 (1964) 2657.
[47] R.C. Bray, in: P.D. Boyer (Ed.), The Enzymes, vol. 12, third edition, Academic Press, New York, 1974, p. 299.
[48] R. Hille, J.H. Kim, C. Hemann, Biochemistry 32 (1993) 3973.
[49] M.S. Mondal, S. Mitra, Biochemistry 33 (1994) 10305.
[50] P. Ilich, R. Hille, J. Phys. Chem. B 103 (1999) 5406.
[51] P. Ilich, R. Hille, J. Am. Chem. Soc. 124 (2002) 6796.
[52] V. Massey, D.E. Edmondson, J. Biol. Chem. 245 (1970) 6596.
[53] N. Wagener, A.J. Pierik, A. Ibdah, R. Hille, H. Dobbek, Proc. Natl. Acad. Sci. U.S.A. 106 (2009) 11055.
[54] R.L. McNaughton, M.E. Helton, M.M. Cosper, J.H. Enemark, M.L. Kirk, Inorg. Chem. 43 (2004) 1625.
[55] C.J. Doonan, N.D. Rubie, K. Peariso, H.H. Harris, S.Z. Knottenbelt, G.N. George, C.G. Young, M.L. Kirk, J. Am. Chem. Soc. 130 (2008) 55.
[56] X.-H. Zhang, Y.-D. Wu, Inorg. Chem. 44 (2005) 1466.
[57] T. Amano, N. Ochi, H. Sato, S. Sakaki, J. Am. Chem. Soc. 129 (2007) 8131.
[58] S. Metz, W. Thiel, J. Am. Chem. Soc. 131 (2009) 14885.
[59] S. Metz, W. Thiel, J. Phys. Chem. B 114 (2010) 1506.
[60] S. Metz, W. Thiel, this issue.
[61] S. Leimkühler, A.L. Stockert, K. Igarashi, T. Nishino, R. Hille, J. Biol. Chem. 279 (2004) 40437.
[62] Y. Yamaguchi, T. Matsumura, K. Ichida, K. Okamoto, T. Nishino, J. Biochem. 141 (2007) 513.
[63] J.M. Pauff, C.F. Hemann, S. Leimkühler, R. Hille, J. Biol. Chem. 282 (2007) 12785.
[64] P. Ilich, R. Hille, Inorg. Chim. Acta 263 (1997) 87.
[65] V. Massey, H. Komai, G. Palmer, G.B. Elion, J. Biol. Chem. 245 (1970) 2837.
[66] J.J. Truglio, K. Theis, S. Leimkühler, R. Rappa, K.V. Rajagopalan, C. Kisker, Structure 10 (2002) 115.
[67] J.M. Pauff, H. Cao, R. Hille, J. Biol. Chem. 284 (2009) 8751.
[68] H. Cao, J.M. Pauff, R. Hille, J. Biol. Chem. 285 (2010) 28044.
[69] J.S. Olson, D.P. Ballou, G. Palmer, V. Massey, J. Biol. Chem. 249 (1974) 4363.
[70] R. Hille, V. Massey, J. Biol. Chem. 261 (1986) 1241.
[71] R. Hille, Biochemistry 30 (1991) 8522.
[72] R. Hille, R.F. Anderson, J. Biol. Chem. 266 (1991) 5608.
[73] L.W. Lim, N. Shamala, F.S. Mathews, D.J. Steenkamp, R. Hamlin, N.h. Xuong, J. Biol. Chem. 261 (1986) 15140.
[74] R.J. Rohlfs, L. Huang, R. Hille, J. Biol. Chem. 270 (1995) 22196.
[75] R. Hille, R.F. Anderson, J. Biol. Chem. 276 (2001) 31193.
[76] T. Nishino, J. Biochem. 116 (1994) 1.
[77] R. Hille, T. Nishino, FASEB J. 9 (1995) 995.
[78] H. Komai, V. Massey, G. Palmer, J. Biol. Chem. 244 (1969) 1692.
[79] V. Massey, C.M. Harris, Biochem. Soc. Trans. 25 (1997) 750.
[80] K.V. Rajagopalan, P. Handler, J. Biol. Chem. 242 (1967) 4097.
[81] M. Kanda, F.O. Brady, K.V. Rajagopalan, P. Handler, J. Biol. Chem. 247 (1972) 765.
[82] D. Barrett, N.A. Davidson, J. Insect Physiol. 21 (1975) 1447.
[83] E.D. Corte, F. Stirpe, Biochem. J. 108 (1968) 349.
[84] F. Stirpe, E.D. Corte, J. Biol. Chem. 244 (1969) 3855.
[85] E.D. Corte, F. Stirpe, Biochem. J. 126 (1972) 739.
[86] W.R. Waud, K.V. Rajagopalan, Arch. Biochem. Biophys. 172 (1976) 354.
[87] M. Nakamura, I. Yamazaki, J. Biochem. 92 (1982) 1279.
[88] J.M. McCord, R.S. Roy, Can. J. Physiol. Pharmacol. 60 (1982) 1346.
[89] J.M. McCord, N. Engl. J. Med. 312 (1985) 159.
[90] O.D. Saugstad, Pediatr. Res. 23 (1988) 143.
[91] C.E. Berry, J.M. Hare, J. Physiol. 555 (2004) 589.
[92] T. Nishino, K. Okamoto, B.T. Eger, E.F. Pai, T. Nishino, FEBS J. 275 (2008) 3278.
[93] C. Vorbach, A. Scriven, M.R. Capecchi, Gene Dev. 16 (2002) 3223.
[94] H.A. Simmonds, S. Reiter, T. Nishino, in: C.R. Scriver, A.L. Beaudet, W.S. Sly, D. Valle (Eds.), Xanthinuria in the Metabolic and Molecular Basis of Inherited Disease, seventh edition, McGraw-Hill, New York, London, 1995, p. 1781.
[95] T. Watanabe, N. Ihara, T. Itoh, T. Fujita, Y. Sugimoto, J. Biol. Chem. 275 (2000) 21789.
[96] K. Ichida, T. Matsumura, R. Sakuma, T. Hosoya, T. Nishino, Biochem. Biophys. Res. Commun. 285 (2001) 1194.
[97] C.A. Woolfolk, J.S. Downard, J. Bacteriol. 130 (1977) 1175.
[98] A.G. Reaume, S.H. Clark, A. Chovnick, Genetics 123 (1989) 503.
[99] G.B. Elion, Science 244 (1989) 41.
[100] J.F. Henderson, M.K.Y. Khoo, J. Biol. Chem. 240 (1965) 3104.
[101] C.T. Caskey, D.M. Ashton, J.B. Wyngaaden, J. Biol. Chem. 239 (1964) 2570.
[102] F. Irreverre, S.H. Mudd, W.D. Heizer, L. Laster, Biochem. Med. 1 (1967) 187.
[103] R.K. Robbins, J. Am. Chem. Soc. 788 (1956) 784.
[104] K. Okamoto, B.T. Eger, T. Nishino, E.F. Pai, T. Nishino, Nucleosides Nucleotides Nucleic Acids 27 (2008) 888.
[105] K. Okamoto, B.T. Eger, T. Nishino, S. Kondo, E.F. Pai, T. Nishino, J. Biol. Chem. 278 (2003) 1848.
[106] A. Fukunari, K. Okamoto, T. Nishino, B.T. Eger, E.F. Pai, M. Kamezawa, I. Yamada, I.N. Kato, J. Pharmacol. Exp. Ther. 311 (2004) 519.
[107] K. Matsumoto, K. Okamoto, N. Ashizawa, T. Nishino, J. Pharmacol. Exp. Ther. (in press), doi:10.1124/jpet.110.174540.
[108] T. Saito, T. Nishino, J. Biol. Chem. 264 (1989) 10015.
[109] J. Hunt, V. Massey, J. Biol. Chem. 267 (1992) 21479.
[110] C.M. Harris, V. Massey, J. Biol. Chem. 272 (1997) 8370.
[111] A.G. Porras, G. Palmer, J. Biol. Chem. 275 (1982) 11617.
[112] E. Garattini, R. Mendel, M.J. Romao, R. Wright, M. Terao, Biochem. J. 372 (2003) 15.
[113] Y. Kuwabara, Y.T. Nishino, K. Okamoto, T. Matsumura, B.T. Eger, E.F. Pai, T. Nishino, Proc. Natl. Acad. Sci. U.S.A. 100 (2003) 8170.
[114] T. Nishino, K. Okamoto, Y. Kawaguchi, H. Hori, K. Igarashi, B.T. Eger, E.F. Pai, T. Nishino, J. Biol. Chem. 280 (2005) 24888.
[115] R. Asai, T. Nishino, T. Matsumura, K. Okamoto, K. Igarashi, E.F. Pai, T. Nishino, J. Biochem. 141 (2007) 525.
[116] J. Bordas, R.C. Bray, C.D. Garner, S. Gutteridge, S.S. Hasnain, Biochem. J. 191 (1980) 499.
[117] J.L. Johnson, B.E. Hainline, K.V. Rajagopalan, J. Biol. Chem. 255 (1980) 1783.
[118] K.V. Rajagopalan, in: M.P. Coughlan (Ed.), Molybdenum and Molybdenum-Containing Enzymes, Pergamon Press, Oxford, 1980, p. 241.
[119] R.C. Wahl, K.V. Rajagopalan, J. Biol. Chem. 257 (1982) 1354.
[120] J.B. Courtright, Genetics 57 (1967) 25.
[121] H.S. Forrest, E. Glassman, H.K. Mitchell, Science 124 (1956) 725.
[122] H.S. Forrest, E.W. Hanley, J.M. Lagowski, Genetics 46 (1961) 1455.
[123] A.M. Bogaart, C.F. Bernini, Biochem. Genet. 19 (1981) 929.
[124] C.K. Warner, V. Finnerty, Mol. Gen. Genet. 184 (1981) 92.
[125] R.C. Wahl, C.K. Warner, V. Finnerty, K.V. Rajagopalan, J. Biol. Chem. 257 (1982) 3958.
[126] C. Scazzocchio, Mol. Gen. Genet. 125 (1973) 147.
[127] C. Scazzocchio, F.B. Holl, A.I. Fogelman, Eur. J. Biochem. 36 (1973) 428.
[128] L. Amrani, J. Primus, A. Glatigny, L. Arcangeli, C. Scazzocchio, V. Finnerty, Mol. Microbiol. 38 (2000) 114.
[129] T. Yamamoto, Y. Moriwaki, S. Takahashi, Z. Tsutsumi, K. Tuneyoshi, K. Matsui, J. Cheng, T. Hada, Metabolism 52 (2003) 1501.
[130] H. Peretz, M.S. Naamati, D. Levartowsky, A. Lagziel, E. Shani, I. Horn, H. Shalev, D. Landau, Mol. Genet. Metab. 91 (2007) 23.
[131] N. Komoto, H. Sezutsu, K. Yukuhiro, Y. Banno, H. Fujii, Insect Biochem. Mol. Biol. 33 (2003) 417.
[132] E. Marin, A. Marion-Poll, Plant Physiol. Biochem. 35 (1997) 369.
[133] A.D. Parry, A.D. Blonstein, M.J. Babiano, P.J. King, R. Horgan, Planta 183 (1991) 237.
[134] K.M. Léon-Kloosterziel, M. Alvarez Gil, G.J. Ruijs, S.E. Jacobsen, N.E. Olszewski, S.H. Schwartz, J.A.D. Zeevaart, M. Koorneef, Plant J. 10 (1996) 655.
[135] F. Llorente, J.C. Oliveros, J.M. Martínez-Zapater, J. Salinas, Planta 211 (2000) 648.
[136] L. Xiong, M. Ishitani, H. Lee, J.K. Zhu, Plant Cell 13 (2001) 2063.
[137] X. Dai, K. Hayashi, H. Nozaki, Y. Cheng, Y. Zhao, Proc. Natl. Acad. Sci. U.S.A. 102 (2005) 3129.
[138] R. Zhong, J. Thompson, E. Ottesen, G.K. Lamppa, Plant J. 63 (2010) 44.
[139] T.W. Stone, H.A. Simmonds, Purines: Basic and Clinical Aspects, vol. 257, Kluwer Academic Press, London, 1991.
[140] K. Ichida, M. Yoshida, R. Sakuma, T. Hosoya, Intern. Med. 37 (1998) 77.
[141] M. Seo, H. Koiwai, S. Akaba, T. Komano, T. Oritani, Y. Kamiya, T. Koshiba, Plant J. 23 (2000) 481.
[142] F. Bittner, M. Oreb, R.R. Mendel, J. Biol. Chem. 276 (2001) 40381.
[143] M. Sagi, C. Scazzocchio, R. Fluhr, Plant J. 31 (2002) 305.
[144] T. Heidenreich, S. Wollers, R.R. Mendel, F. Bittner, J. Biol. Chem. 280 (2005) 4213.
[145] S. Wollers, T. Heidenreich, M. Zarepour, D. Zachmann, C. Kraft, Y. Zhao, R.R. Mendel, F. Bittner, J. Biol. Chem. 283 (2008) 9642.
[146] S. Leimkühler, W. Klipp, J. Bacteriol. 181 (1999) 2745.
[147] S. Leimkühler review, this issue.
[148] R.R. Mendel, G. Schwarz review, this issue.
[149] H. Dobbek, L. Gremer, O. Meyer, R. Huber, Proc. Natl. Acad. Sci. U.S.A. 96 (1999) 8884.
[150] E. Garattini, M. Fratelli, M. Terao, Cell. Mol. Life Sci. 65 (2008) 1019.
[151] M. Terao, M. Kurosaki, M.M. Barzago, M. Fatelli, R. Bagnati, A. Bastone, C. Guidici, E. Scanziani, A. Mancuso, C. Tiveron, E. Garattini, Mol. Cell. Biol. 29 (2009) 357.
[152] M. Kurosaki, M. Terao, M.M. Barzago, A. Bastone, D. Bernardinello, M. Salmona, E. Garattini, J. Biol. Chem. 279 (2004) 50482.
[153] M. Seo, A.J.M. Peeters, H. Koiwai, T. Oritani, A. Marion-Poll, J.A.D. Zeevart, M. Koornneef, Y. Kamiya, T. Koshiba, Proc. Natl. Acad. Sci. U.S.A. 97 (2000) 12908.
[154] T. Hoff, G.I. Frandsen, A. Rocher, J. Mundy, Biochim. Biophys. Acta 1398 (1998) 397.
[155] M. Seo, H. Aoki, H. Koiwai, T.Y. Kamiya, E. Nambara, T. Koshiba, Plant Cell Physiol. 45 (2004) 1694;
M. Seo, H. Aoki, H. Koiwai, T.Y. Kamiya, E. Nambara, T. Koshiba, Plant Cell Physiol. 97 (2000) 12908.
[156] E. Zdunek-Zastocka, Plant Physiol. Biochem. 46 (2008) 19.
[157] J.F. Alfaro, J.P. Jones, J. Org. Chem. 23 (2008) 9469.
[158] N.A. Turner, W.A. Doyle, A.M. Ventom, R.C. Bray, Eur. J. Biochem. 232 (1995) 646.
[159] R.A. Torres, K.R. Korzekwa, D.R. McMasters, C.M. Fandozzi, J.P. Jones, J. Med. Chem. 50 (2007) 4642.
[160] J.F. Alfaro, C.A. Joswing-Jones, W. Ouyang, J. Nicols, G.J. Crouch, J.P. Jones, Drug Metab. Dispos. 37 (2009) 2393.
[161] C. Kisker, H. Schindelin, A. Pacheco, W.A. Wehbi, R.M. Garrett, K.V. Rajagopalan, J.H. Enemark, D.C. Rees, Cell 91 (1997) 973.
[162] N. Schrader, K. Fischer, K. Theis, R.R. Mendel, G. Schwarz, C. Kisker, Structure 11 (2003) 1251.
[163] T. Eilers, G. Schwarz, H. Brinkmann, C. Witt, T. Richter, J. Nieder, B. Koch, R. Hille, R. Hänsch, R.R. Mendel, J. Biol. Chem. 276 (2001) 46989.

[164] G.J. Workun, K. Moquin, R.A. Rothery, J.H. Weiner, Microbiol. Mol. Biol. Rev. 72 (2008) 228.
[165] C. Hemann, B.L. Hood, M. Fulton, R. Hänsch, G. Schwarz, R.R. Mendel, M.L. Kirk, R. Hille, J. Chem. Soc. 127 (14) (2005) 16587.
[166] J.L. Johnson, K.V. Rajagopalan, J. Biol. Chem. 252 (1977) 2017.
[167] E. Karakas, H.L. Wilson, T.N. Graf, S. Xiang, S. Jaramillo-Busquets, K.V. Rajagopalan, J. Biol. Chem. 280 (2005) 33506.
[168] R.M. Garrett, K.V. Rajagpalan, J. Biol. Chem. 271 (1996) 7387.
[169] G.N. George, R.M. Garrett, R.C. Prince, K.V. Rajagpalan, J. Am. Chem. Soc. 118 (1996) 8588.
[170] G.N. George, R.M. Garrett, R.C. Prince, K.V. Rajagpalan, Inorg. Chem. 43 (2004) 8456.
[171] M.T. Lamy, S. Gutteridge, R.C. Bray, Biochem. J. 185 (1980) 397.
[172] J.A. Qiu, H.L. Wilson, M.J. Pushie, C. Kisker, G.N. George, K.V. Rajagopalan, Biochemistry 49 (2010) 3989.
[173] M.L. Kirk, C. Young review, this issue.
[174] S. Leimkühler, K.V. Rajagopalan, J. Biol. Chem. 276 (2001) 1837.
[175] M.A. Pietsch, M.B. Hall, Inorg. Chem. 35 (1996) 1273.
[176] L.M. Thomson, M.B. Hall, J. Am. Chem. Soc. 123 (2001) 3995.
[177] A.K. Rappé, W.A. Goddard, Nature 285 (1980) 311.
[178] R. Hille, Biochim. Biophys. Acta 1184 (1994) 143.
[179] K. Peariso, R.L. McNaughton, M.L. Kirk, J. Am. Chem. Soc. 124 (2002) 9006.
[180] M.S. Brody, R. Hille, Biochim. Biophys. Acta 1253 (1995) 133.
[181] M.S. Brody, R. Hille, Biochemistry 38 (1999) 6668.
[182] H.L. Wilson, K.V. Rajagopalan, J. Biol. Chem. 279 (2004) 15105.
[183] R.M. Garrett, J.L. Johnson, T.N. Graf, A. Feigenbaum, K.V. Rajagopalan, Proc. Natl. Acad. Sci. U.S.A. 95 (1998) 6394.
[184] S. Strickland, G. Palmer, V. Massey, J. Biol. Chem. 250 (1975) 4048.
[185] S. Bailey, T. Rapson, K. Johnson-Winters, A.V. Astashkin, J.H. Enemark, J. Biol. Chem. 284 (2009) 2053.
[186] E.P. Sullivan, J.T. Hazzard, G. Tollin, J.H. Enemark, Biochemistry 32 (1993) 12465.
[187] A. Pacheco, J.T. Hazzard, G. Tollin, J.H. Enemark, J. Biol. Inorg. Chem. 4 (1999) 390.
[188] K. Johnson-Winters, A.R. Nordstrom, S. Emesh, A.V. Astashkin, A. Rajapakshe, R.E. Berry, G. Tollin, J.H. Enemark, Biochemistry 49 (2010) 1290.
[189] C. Feng, R.V. Kedia, J.T. Hazzard, J.K. Hurley, G. Tollin, J.H. Enemark, Biochemistry 41 (2002) 5816.
[190] R. Codd, A.V. Astashkin, A. Pacheco, A.M. Raitsimring, J.H. Enemark, J. Biol. Inorg. Chem. 7 (2002) 338.
[191] C. Feng, H.L. Wilson, J.K. Hurley, J.T. Hazzard, G. Tollin, K.V. Rajagopalan, J.H. Enemark, J. Biol. Chem. 278 (2003) 2913.
[192] C. Feng, H.L. Wilson, J.K. Hurley, J.T. Hazzard, G. Tollin, K.V. Rajagopalan, J.H. Enemark, Biochemistry 42 (2003) 12235.
[193] C. Feng, H.L. Wilson, G. Tollin, A.V. Astashkin, J.T. Hazzard, K.V. Rajagopalan, J.H. Enemark, Biochemistry 44 (2005) 13734.
[194] S.J. Elliott, A.E. McElhaney, C. Feng, J.H. Enemark, F.A. Armstrong, J. Am. Chem. Soc. 124 (2002) 11612.
[195] R. Dronov, D.K. Kurth, H. Möhwald, R. Spricigo, S. Leimkühler, U. Wollenberger, K.V. Rajagopalan, F.W. Scheller, F. Lisdat, J. Am. Chem. Soc. 130 (2008) 1122.
[196] S.H. Speck, W.H. Koppenol, J.K. Dethmers, N. Osheroff, E. Margoliash, K.V. Rajagopalan, J. Biol. Chem. 256 (1981) 7394.
[197] R. Hänsch, C. Lang, E. Riebeseel, R. Lindigkeit, A. Gessler, H. Rennenberg, R.R. Mendel, J. Biol. Chem. 281 (2006) 6884.
[198] R. Byrne, R. Hänsch, R.R. Mendel, R. Hille, J. Biol. Chem. 284 (2009) 34579.
[199] G. Brychkova, Z. Xia, G. Yang, Z. Yesbergenova, Z. Zhang, O. Davydov, R. Fluhr, M. Sagi, Plant J. 50 (2007) 696.
[200] R. Hänsch, C. Lang, H. Rennenberg, R.R. Mendel, Plant Biol. 9 (2007) 589.
[201] A.M. Raitsimring, A. Pacheco, J.H. Enemark, J. Am. Chem. Soc. 120 (1998) 11263.
[202] A.V. Astashkin, M.L. Mader, A. Pacheco, J.H. Enemark, A.M. Raitsimring, J. Am. Chem. Soc. 122 (2000) 5294.
[203] A.V. Astashkin, A.M. Raitsimring, C. Feng, J.L. Johnson, K.V. Rajagopalan, J.H. Enemark, J. Am. Chem. Soc. 124 (2002) 6109.
[204] S.P. Cramer, J.L. Johnson, K.V. Rajagopalan, Biochem. Biophys. Res. Commun. 91 (1979) 434.
[205] S.D. Garton, R.M. Garrett, K.V. Rajagopalan, M.K. Johnson, J. Am. Chem. Soc. 119 (1997) 2590.
[206] A.V. Astashkin, C. Feng, A.M. Raitsimring, J.H. Enemark, J. Am. Chem. Soc. 127 (2005) 502.
[207] R.C. Bray, M.T. Lamy, S. Gutteridge, T. Wilkinson, Biochem. J. 201 (1982) 231.
[208] A.M. Raitsimring, A.V. Astashkin, C. Feng, H.L. Wilson, K.V. Rajagopalan, J.H. Enemark, Inorg. Chim. Acta 361 (2008) 941.
[209] R.C. Bray, M.T. Gutteridge, M.T. Lamy, S.T. Wilkinson, Biochem. J. 211 (1983) 227.
[210] C.J. Doonan, H.L. Wilson, B. Bennett, R.C. Prince, K.V. Rajagopalan, G.N. George, Inorg. Chem. 47 (2008) 2033.
[211] E.L. Klein, A.V. Astashkin, D. Ganyushev, C. Riplinger, K. Johnson-Winters, F. Neese, J.H. Enemark, Inorg. Chem. 48 (2009) 4743.
[212] A. Rajapakshe, K. Johnson-Winters, A.R. Nordstrom, K.T. Meyers, S. Emesh, A.V. Astashkin, J.H. Enemark, Biochemistry 49 (2010) 5154.
[213] A.V. Astashkin, K. Johnson-Winters, E.L. Klein, C. Feng, H.L. Wilson, K.V. Rajagopalan, A.M. Raitsimring, J.H. Enemark, J. Am. Chem. Soc. 130 (2008) 8471.
[214] L.P. Solomonson, M.J. Barber, Annu. Rev. Plant Mol. Biol. 41 (1990) 225.
[215] W.H. Campbell, Annu. Rev. Plant Mol. Biol. 50 (1999) 277.
[216] W.H. Campbell, Cell. Mol. Life Sci. 58 (2001) 194.
[217] Y. Kubo, H. Nakagawa, J. Biol. Chem. 263 (1988) 19684.
[218] K. Fischer, G.G. Barbier, H.-J. Hecht, R.R. Mendel, W.H. Campbell, G. Schwarz, Plant Cell 17 (2005) 1167.
[219] A.C. Cannons, M.J. Barber, L.P. Solomonson, J. Biol. Chem. 268 (1993) 3268.
[220] R.C.E. Durley, F.S. Mathews, Acta Crystallogr. D 52 (1996) 65.
[221] G. Lu, W.H. Campbell, G. Schneider, Y. Lindquist, Structure 2 (1994) 809.
[222] S.P. Cramer, L.P. Solomonson, M.W.W. Adams, L.E. Mortenson, J. Am. Chem. Soc. 106 (1984) 1467.
[223] G.N. George, J.A. Mertens, W.H. Campbell, J. Am. Chem. Soc. 121 (1999) 9730.
[224] R.H. Holm, J.P. Donahue, Polyhedron 12 (1993) 571.
[225] L. Skipper, W.H. Campbell, J.A. Mertens, D.J. Lowe, J. Biol. Chem. 276 (2001) 26995.
[226] K. Ratnam, N. Shiraishi, W.H. Campbell, R. Hille, J. Biol. Chem. 270 (1995) 24067.
[227] K. Ratnam, N. Shiraishi, W.H. Campbell, R. Hille, J. Biol. Chem. 272 (1997) 2122.
[228] J.A. Mertens, N. Shiraishi, W.H. Campbell, Plant Physiol. 123 (2000) 743.
[229] J.A. Mertens, W.H. Campbell, L.D.J. Skipper, D.J. Lowe, in: S. Ghisla, P. Kroneck, P. Macheroux, H. Sund (Eds.), Flavins and Flavoproteins, Rudolph Weber, Berlin, 1999, p. 131.
[230] I. Sherameti, S.K. Sopory, A. Trebicka, T. Pfannschmidt, R. Oelmüller, J. Biol. Chem. 277 (2002) 46594.
[231] J.L. Huber, S.C. Huber, W.H. Campbell, M.G. Redinbaugh, Arch. Biochem. Biophys. 296 (1992) 58.
[232] M. Bachmann, N. Shiraishi, W.H. Campbell, B.-C. Yoo, A.C. Harmon, S.C. Huber, Plant Cell 8 (1996) 505.
[233] P. Douglas, G. Moorhead, Y. Hong, N. Morrice, C. MacKintosh, Planta 206 (1996) 435.
[234] G. Moorhead, P. Douglas, N. Morrice, M. Scarabel, A. Aitken, C. MacKintosh, Curr. Biol. 6 (1996) 1104.
[235] W. Shen, S.C. Huber, Plant Cell Physiol. 47 (2006) 764.
[236] I. Lambeck, J.-C. Chi, S. Krizowski, S. Mueller, N. Mehlmer, M. Teige, K. Fischer, G. Schwarz, Biochemistry 49 (2010) 8177.
[237] B. Wahl, D. Reichmann, D. Niks, N. Krompholz, A. Havemeyer, B. Clement, T. Meßerschmidt, M. Rothkegel, H. Biester, R. Hille, R.R. Mendel, F. Bittner, J. Biol. Chem. 285 (2010) 37847.
[238] S.G. Kozmin, P. Leroy, Y.I. Pavlov, R.M. Schaaper, Mol. Microbiol. 68 (2008) 51.
[239] J. Kotthaus, B. Wahl, A. Havemeyer, J. Kotthaus, D. Schade, F. Bittner, R.R. Mendel, B. Clement, Biochem. J., doi:10.1042/BJ20100960, in press.
[240] A. Havemeyer, S. Gruenewald, B. Wahl, F. Bittner, R.R. Mendel, P. Erdélyi, J. Fischer, B. Clement, Drug Metab. Dispos. 38 (2010) 1917.
[241] S. Da Cruz, I. Xenarios, J. Langridge, F. Vilbois, P. Parone, J. Martinou, J. Biol. Chem. 278 (2003) 41566.
[242] M. Islinger, G.H. Lüers, K.W. Li, M. Loos, A. Völkl, J. Biol. Chem. 282 (2007) 23055.
[243] V. Anantharaman, L. Aravind, FEMS Microbiol. Lett. 207 (2002) 55.
[244] K. Okamoto, Y. Kawaguchi, B.T. Eger, E.F. Pai, T. Nishino, J. Am. Chem. Soc. 132 (2010) 17080.